IEEE Access
Multidisciplinary | Rapid Review | Open Access Journal

Received 25 April 2023, accepted 22 May 2023, date of publication 1 June 2023, date of current version 12 June 2023.

Digital Object Identifier 10.1109/ACCESS.2023.3281488

RESEARCH ARTICLE

Machine Learning-Based Adaline Neural PQ Strategy for a Photovoltaic Integrated Shunt Active Power Filter

ASMAE AZZAM JAI AND MOHAMMED OUASSAID, (Senior Member, IEEE)
Engineering for Smart and Sustainable Systems Research Center, Mohammadia School of Engineers, Mohammed V University in Rabat, Rabat 10090, Morocco
Corresponding author: Asmae Azzam Jai (azzam@emi.ac.ma)

ABSTRACT This paper introduces novel techniques based on Machine Learning (ML) algorithms for a Photovoltaic integrated Shunt Active Power Filter performance improvement. The first goal is to design an efficient maximum power point tracking MPPT strategy in order to harness the largest amount of energy possible. Thereby, a new hybrid Support Vector Machine Regression Perturb and Observe (SVM regression-P&O) algorithm is proposed. The SVM block improves the tracking speed by predicting an initial duty cycle, whereas a small fixed-step P&O algorithm ensures a high MPPT accuracy. The second purpose is to upgrade harmonics detection by exploiting the characteristics of intelligent learning of Adaline combined with ML algorithm. Therefore, a novel SVM regression-Adaline PQ strategy is designed. The SVM block generates the predicted initial weights of Adaline, thus ensuring fast identification of the DC active power component. In addition, the ability of this design to work with a small learning rate parameter allows an accurate harmonics extraction in contrast with the Adaptive Adaline technique where the performances are highly dependent on the chosen learning rate parameter. A comparative analysis of various ML models are carried out in order to get the best output prediction for each SVM regression block. Simulations have been performed to confirm the supremacy of the new strategies over intelligent and classical techniques. Finding exhibits a significant decrease of PV energy losses (up to 99%), a minor overshoot with an impressively decrease of the harmonics extraction's response time (up to 98.8%), and a PVSAPF power quality enhancement under online intermittent weather conditions and variable nonlinear load.

INDEX TERMS Machine learning, support vector machine regression, photovoltaic integrated shunt active power filter, maximum power point tracking, harmonics identification.

I. INTRODUCTION

Renewable energy (RE) resources have received increased global interest in the prior 20 years, and became a promising alternative toward a sustainable future [1], [2]. From one viewpoint, there is a worldwide concern and a large pressure over security for the energy supply to reach a higher level owing to the concentrated feature of oil reserves and political instability in countries with the greatest deposits. On the other, the burning of fossil fuel in conventional electrical power generation systems is considered the main cause of CO2 emissions in the world [4], contributing to Greenhouse Gas emissions and global climate change. The Intergovernmental Panel on Climate Change (IPCC) predicts a global increase to 4.5°C and 900 ppm CO2 by 2100 [5]. As a result, to address these problems, government policies in many countries have drawn out plans to shift towards electricity production from renewable energy [6], ensuring further market certitude as well as less air pollution. In [7], the global CO2 emission related to the energy production sector gets to 33 gigatonnes (Gt) in 2018 and stabilizes in 2019 despite a global economic increase of 2.9%. This level's stabilization was explained mainly by the proliferation of renewable energies in the electricity production sector.

Solar photovoltaic (PV) has become a cost-competitive technology [8] with a significant cost reduction. Between

The associate editor coordinating the review of this manuscript and approving it for publication was Kaushik Mukherjee.

2020 and 2021, there was a 12.3% ($0.13/W) reduction in utility-scale PV system cost benchmarks [9]. This green technology has also shown exponential growth throughout the last decade [10]. From 2011 to 2021, global PV spreading increased from 72 GW to 843 GW [11], [12]. In power systems, PV panels can be classified into two main types, namely the grid-connected system (on-grid), and the standalone systems (off- grid) [13]. In the 'off-grid' systems, PV works independently from the ac grid and uses storage devices to accumulate the excess energy for later consumption. However, batteries bank have shown to be high-cost devices with relatively low efficiency, making the usage of standalone systems relatively expensive [14]. Meanwhile, in the 'on-grid' systems, PV panels supply power to the utility grid and the use of a batteries bank is not required. Nevertheless, this PV system integration into the existing grid causes many power quality issues (particularly Harmonic distortions and reactive power) [15].

Ensuring the power quality has become a vital task in power distribution systems, owing to the jeopardizing effects of harmonic currents under the increased use of nonlinear loads [16]. Harmonics distortion causes several issues in the surrounding power equipment such as oscillation and overvoltage in the electrical power system, additional loss and voltage drop in transformers and motors, and wrong tripping of protection hardware [17]. Within this context, conventional passive power filters have been installed to upgrade the power quality in the polluted power system. Nevertheless, despite their simplicity and their low cost, the passive power filter still has several drawbacks such as large size, fixed harmonics tuning, and a specific reactive compensation. Therefore, in order to address these issues, the shunt active power filters (SAPF) take the place of the passive ones and are considered the newest technology and the most reliable devices owing to their ability to improve power factor, mitigate harmonics, and work under various operating conditions [18], [19], [20].

The combination of the PV system with SAPF constitutes a multifunctional system. Indeed, the PVSAPF system ensures PV active power injection into the grid and overcomes the PV on-grid issues by enhancing power quality. In this work PVSAPF system is studied under a variable operating condition of the nonlinear load, and/or changing climatic conditions, using two new methods of control based on machine learning and artificial intelligence.

On one hand, the maximization of the power extraction from the photovoltaic arrays is vital for optimal PV-SAPF system exploitation. PV panels exhibit non-linear current-voltage characteristics with a unique point named maximum power point (MPP) for each specific climatic condition [21]. In this regard, it is necessary to design an effective maximum power point tracking MPPT strategy in order to ensure a ceaseless PV maximum power generation under various environmental conditions. Numerous MPPT algorithms have been presented in the literature. These strategies can be classified as conventional, novel, and hybrid ones [22]. The core features sought in all developed MPPT strategies are a good tracking speed, better accuracy, and a low power ondulation under varying weather conditions with low computation burdens and implementation cost [23]. The Perturbation and Observation (P&O) and the incremental conductance (INC) [24] algorithms are still the most common techniques employed for commercial applications, thanks to their simplicity in implementation, and their good performance under constant environmental conditions. Nevertheless, these conventional strategies show poor performances and weak adaptation under permanent variations in the weather [25]. In [26], the tracking speed can be improved by using a large step size but with the penalty of providing additional power fluctuations at MPP. On the other hand, a small step size upgrades the steady state response by reducing remarkably the power oscillations but slows up the response time of MPPT. In order to meet this challenge, variable step-based MPPT algorithms have been introduced in [27]. The authors proposed the derived dP/dV values and scaling factor to generate various step sizes of the incremental conductance method (DVS-INC), ensuring the trade-off between low power oscillation and high tracking speed. Another variable step algorithm using intelligence artificial has been designed in [28]. The study proposes an enhanced MPPT strategy combining a Fuzzy Logic Controller FLC with incremental conductance algorithm. Five step sizes are generated in accordance with five areas of the fuzzy controller inputs. However, this technique has the disadvantage that the performances depend strongly on the chosen step size, along with the FLC limitation, which depends on experience for rules and membership functions determination [29]. Another work in [30] presents a review of various studies over the last six years using Artificial Neural Networks (ANN) based MPPT algorithms. This Intelligent controller gives better static and dynamic performances as further is data gathered. Nonetheless, the major disadvantage of the ANN controller is the high-cost solution that it presents owing to the increased computational load that it requires. In recent years, Machine Learning classification techniques are progressing at a very fast cadence, and are widely used for solar irradiance forecasting [31], and electrical system fault detection [32]. Nonetheless, there are comparatively few studies using machine learning regression problems related to maximum power extraction MPPT in the PV-SAPF system. In this work, a novel hybrid Support Vector Regression-P&O MPPT algorithm has been designed, in order to afford an optimized solution ensuring a compromise between cost, tracking speed, and accuracy of the MPPT strategy.

On the other hand, harmonics detection is considered a crucial step, in the PV SAPF system control, facing the power quality issues, caused by the nonlinear load utilization as well as the PV power injection [33]. Several harmonic extraction strategies have been proposed such as Fourier analysis-based techniques in the frequency domain [34], dq theory and instantaneous power theory-based algorithms

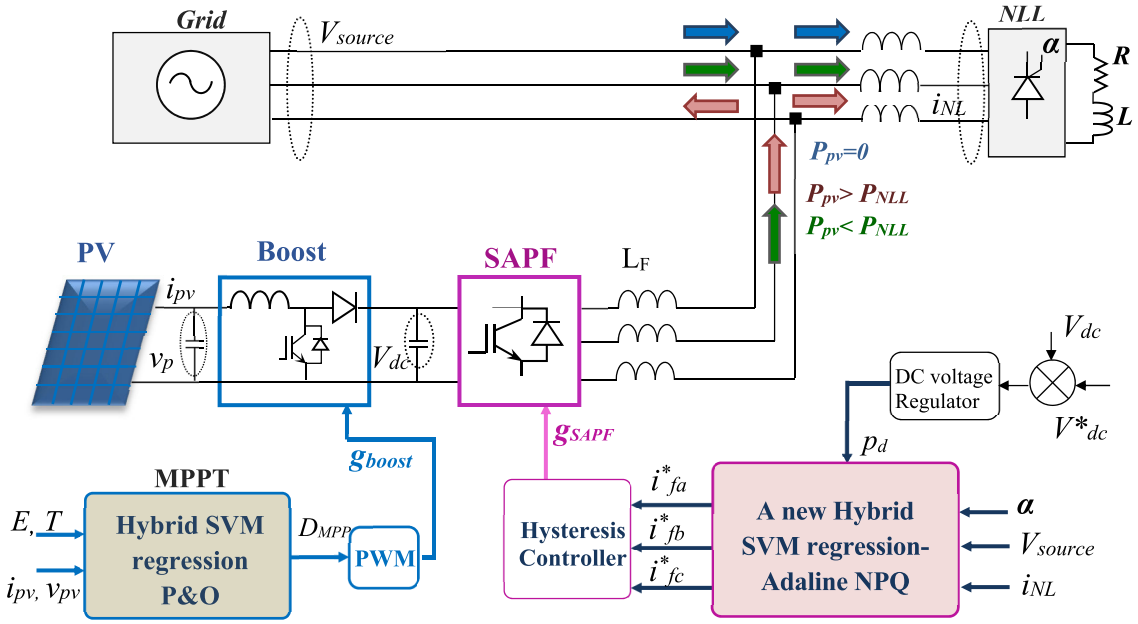

FIGURE 1. Circuit diagram the studied PV-SAPF system.

in the time domain [35], and artificial intelligence-based approaches [36].

In the frequency-based techniques, the computational burden caused by the needed time in collecting adequate samples gives poor dynamic performances in comparison with the time domain strategies [37]. These latter offer better performance in terms of response time, but lack accuracy particularly under varying loads [38]. Hence, Adaline-based neural network techniques have been designed in order to overcome the limitations of classical detection strategies, thanks to its intelligent learning and fast training characteristics [38]. Nevertheless, this neural strategy has limitations as well. Indeed, the use of a high learning rate parameter in the Adaline-based technique improves the tracking speed of harmonics detection, but with the penalty of providing oscillations in the steady state response. Moreover, a small learning rate parameter upgrades the steady state response by reducing remarkably fluctuations, but slows up the response time of harmonics extraction [39]. Therefore, this paper gives a significant improvement in harmonics detection and presents a new hybrid Support Vector Regression-Adaline neural PQ strategy for the PVSAPF system.

The contribution of this paper reposes on the main features mentioned below

- A novel design of a hybrid SVM regression-P&O MPPT is adopted and compared to Fuzzy MPPT and P&O MPPT algorithms.
- A novel design of a hybrid SVM Adaline NPQ strategy for harmonics extraction is developed and compared to the intelligent Neural Adaline PQ strategy and to the classical instantaneous PQ method using the Low Pass Filter (LPF).
- The proposed hybrid SVM-P&O MPPT provides an accurate and fast MPPT response with low ondulation under abrupt changes in the weather parameters.
- The proposed SVM regression-Adaline NPQ strategy offers an important advance in DC active power component extraction under a sudden NLL parameters variation.
- The combination of both proposed new algorithms presents an efficient PVSAPF's control strategy in terms of static and dynamic performance under a variable operating condition of the nonlinear load and/or changing climatic parameters.

The article is organized as follows. Section II describes the PVSAPF system configuration and details the ε-SVR support vector regression algorithm. The design of the SVM-P&O MPPT and hybrid SVM Adaline NPQ control strategies are described in Section III and Section IV, respectively. The simulation results are discussed in Section IV. Finally, Section V concludes the article.

II. PVSAPF SYSTEM CONFIGURATION AND ε-SVR SUPPORT VECTOR REGRESSION ALGORITHM

A. PHOTOVOLTAIC SHUNT ACTIVE POWER FILTER SYSTEM CONFIGURATION

The proposed block diagram of the SAPF coupled PV panels system is shown in Figure 1. As indicated, the power transit of the whole studied system can be categorized, according to the generated PV active power Ppv, into three phases:

- During the concentrated sunshining period ($Ppv > P_{NLL}$), the system supplies power to the nonlinear loads from the PV panels and transfers the active power surplus to the grid.

- When the sunshine is not sufficient ($Ppv < P_{NLL}$), the nonlinear load is fed from both the PV panels and ac grid.

- At night, during the absence of photovoltaic energy production ($Ppv = 0$), the ac grid provides all the electrical power demand to the nonlinear load. Further, the PVSAPF system affords simultaneously reactive power compensation and harmonics current filtering in all these three phases.

The proposed system controller consists of four principal blocks:

- MPPT control block, integrated in the boost converter, for maximum PV power extraction.
- Compensating currents control block for reference currents generation.
- DC bus voltage control block which is used to keep the capacitor voltage at its reference value.
- The hysteresis controller based current control block for generating the switching signals g_{SAPF} to three-phase inverter based the shunt active power filter.

B. ε-SVR ALGORITHM

Designed by Cortes and Vapnik in 1995, Support Vector Regression (SVR) is a supervised and non-parametric learning technique, widely used in regression problems. It gives high learning performance in nonlinear problems even with complex distributed data. The SVR algorithm is be described as following [40].

Consider the sample set of training data:

$$T = \{(x_1, y_1), \ldots, (x_l, y_l)\} \quad (x_i \in \mathbb{R}^N, y_i \in \mathbb{R}, i = 1, \ldots, l) \tag{1}$$

where x_i represents the N-dimensional input vector and y_i the corresponding target value.

Linear SVR function is estimated as the following equation:

$$f(x) = \langle w, \phi(x) \rangle + b \quad \phi : \mathbb{R}^N \to F; w \in F \tag{2}$$

where $\langle , \rangle$ designates the dot product in the feature space F, w the weight vector, $\phi(x)$ the nonlinear mapping data and b the intercept vector of hyperplane $f(x)$. In order to find the optimal regression function, the coefficients w and b can be determined by solving the convex optimization problem, expressed as follows:

$$Min \frac{1}{2} \| w \|^2 + C \sum_{i=1}^{N} (\xi_i + \xi_i^*) \tag{3}$$

$$ST : \begin{cases} y_i - w^T \phi(x_i) - b \leq \varepsilon + \xi_i^* \\ w^T \phi(x_i) + b - y_i \leq \varepsilon + \xi_i \\ \xi_i^*, \xi_i \geq 0 \end{cases} \tag{4}$$

where ε is the insensitive error margin, and C the penalty factor which ensures the compromise between training error reduction and the complexity of SVM model (flatness of the function) [41], [42]. ξ_i and ξ_i^* are slack variables which indicate the absolute deviances above and below the insensitive error margin ε, respectively.

This convex optimization problem can be reconstructed as a Lagrangian function, as follows:

$$\begin{aligned} L = \frac{1}{2} \|w\|^2 + C \sum_{i=1}^{l} (\xi_i + \xi_i^*) - \sum_{i=1}^{l} (\xi_i \delta_i + \xi_i^* \delta_i^*) \\ - \sum_{i=1}^{l} \sigma_i [\xi_i + \varepsilon + y_i - (w, \phi(x_i)) - b] \\ - \sum_{i=1}^{l} \sigma_i^* [\xi_i^* + \varepsilon - y_i + (w, \phi(x_i)) + b] \end{aligned} \tag{5}$$

where $\sigma_i, \sigma_i^*, \delta_i, \delta_i^*$ are Lagrangian multipliers.

From the partial derivative of eq. (5), in one hand the obtained weight vector can be expressed as [43]:

$$w = \sum_{i=1}^{n} (\sigma_i - \sigma_i^*) \phi(x_i) \tag{6}$$

Additionally, the optimization problem is formulated as follows:

$$\begin{aligned} Max - \frac{1}{2} \sum_{i=1}^{n} (\sigma_i - \sigma_i^*) (\sigma_j - \sigma_j^*) K(x_i, x_j) \\ - \varepsilon \sum_{i=1}^{n} (\sigma_i + \sigma_i^*) + \sum_{i=1}^{n} y_i (\sigma_i - \sigma_i^*) \end{aligned} \tag{7}$$

$$ST : \begin{cases} \sum_{i=1}^{N} (\sigma_i + \sigma_i^*) = 0 \\ \sigma_i, \sigma_i^* \in [0, C] \end{cases} \tag{8}$$

where $K(x_i, x_j) = \phi(x_i) . \phi(x_j)$ is kernel function which satisfy the Mercer condition.

Substitute equation (6) into equation (2), the final obtained regression function can be written as follows:

$$\begin{aligned} f(x) &= \sum_{i=1}^{n} (\sigma_i - \sigma_i^*) \phi^T(x_i) \phi(x) + b \\ &= \langle w, \phi(x) \rangle + b = \sum_{i=1}^{N} \beta_i K(x_i, x) + b \end{aligned} \tag{9}$$

Several kernel functions have demonstrated their great ability to improve SVR performance in the literature [44], [45]. In this study, Linear kernel function, Gaussian kernel function, Quadratic kernel function and Cubic kernel function are used [46].

In addition, a suitable choice of Hyperparameter optimization is vital for optimal performance of the ?-SVR technique [47]. The Grid search, the Random search and the Bayesian optimization are the most popular ones. In this study, the appropriate kernel function and the Hyperparameter optimization method are chosen by taking into consideration the following comparing statistical criteria [48]: Root

mean square errors (RMSE), mean absolute errors (MAE) and determination coefficient (R2).

III. THE DESIGN OF THE SVM-P&O MPPT ALGORITHM

A. METHODOLOGY

The SVM regression model used in the proposed MPPT strategy is set to T_{MPP}= *{(x1,y1),……, (xn, yn)}* where x_j is the input sample comprising two features *(E(j),T(j));* $j = 1 \ldots n$ and y_j is output sample of SVM regression block predicting duty cycle $D_{ML}(j)$ of the boost converter. The training data set, represented in Figure 2 is collected from the simulation history of the PV system under varying irradiance and temperature levels.

Referring to Figure 3 which illustrates an example of PV curves under two temperature levels (45°C and 5°C), and to the improved MPPT model detailed in Figure 4, the proposed SVM regression-P&O algorithm can be described as follows: At the first stage, the SVM regression block predicts an initial duty cycle D_{0-ML} according to irradiance E and temperature T levels of the PV panel. The corresponding PWM is sent to the boost converter, thereby, the output active power of PV gets speedily close to MPP.

$$D_{0-MPP} = D_{0-ML} \tag{10}$$

The process is then switched to P&O algorithm using a small fixed step $\Delta D_{P\&O}$ in order to accurately track the MPP.

$$D_{MPP}(k) = D_{MPP}(k-1) \pm \Delta D_{P\&O} \tag{11}$$

When varying parameters E and/or T, the algorithm switches back to the SVM regression model which generates a new predicted output D_{ML} *(k)*. The difference between the current predicted SVM output D_{ML} *(k)* and the last predicted SVM output D_{ML} *(k-1)* is calculated and added to the last duty cycle D_{MPP}*(k-1)*. Thus, the new $D_{MPP}(k)$ is formulated and accordingly will be situated close to the novel MPP.

$$\Delta D_{ML} = D_{ML}(k) - D_{ML}(k-1) \tag{12}$$

$$D_{MPP}(k) = D_{MPP}(k-1) + \Delta D_{ML} \tag{13}$$

After that, if ΔD_{ML}= *0*(this means the output of the SVM regression block does not change: E and $T$are constant), the P&O algorithm with a small fixed step is started again and continues until the MPP is followed.

Introducing the switching function $\lambda \in \{0, 1\}$ and combining Equations (11), (12), and (13) yields to:

$$D_{MPP}(k) = D_{MPP}(k-1) + (1-\lambda)\Delta D_{ML} \pm \lambda \Delta D_{P\&O} \tag{14}$$

where λ= *1* when E and T are constant, and λ= *0* when E and/or T varies. The flowchart of proposed SVM regression-P&O algorithm is depicted in Figure 5.

B. SVM REGRESSION BASED DUTY CYCLE PREDICTION

In order to select the appropriate kernel function, along with Hyperparameter optimization method to get the best duty cycle prediction by SVM regression model, four kernel functions are tested: Linear R, Gaussian G, Quadratic Q and Cubic C basis function kernel.

The SVM regression model is trained for each kernel function with three Hyperparameter optimization methods: Bayesian optimization B, Grid search G, Random search R. Therefore twelve models have been evaluated and the training results are grouped and presented by the predicted response versus record number and the predicted versus actual plot in Figure 6 and Figure 7 respectively.

In addition, the performance of each model are evaluated according to the statistical criteria cited in Section II/Subsection B.

A comprehensive performance comparison is presented in Table 1. Referring to these training and evaluating results, it is clear that Gaussian kernel function with Random search Hyperparameter optimization method (G-R) gives the best duty cycle prediction. Consequently, G-R is selected and will be used throughout the rest of this work for SVM regression-P&O MPPT algorithm.

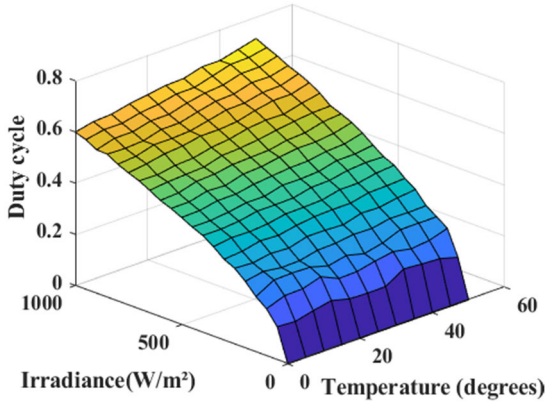

FIGURE 2. Duty cycle, T, E.

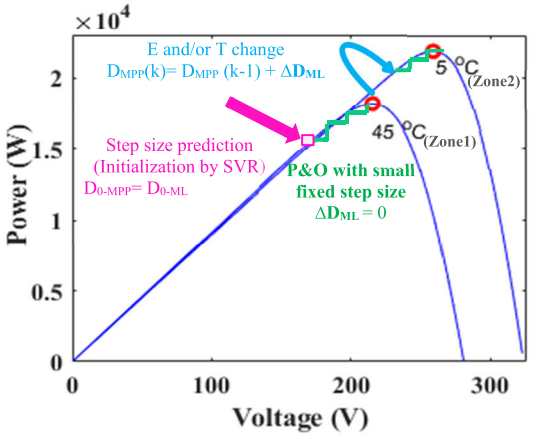

FIGURE 3. SVM regression-P&O MPP tracking method.

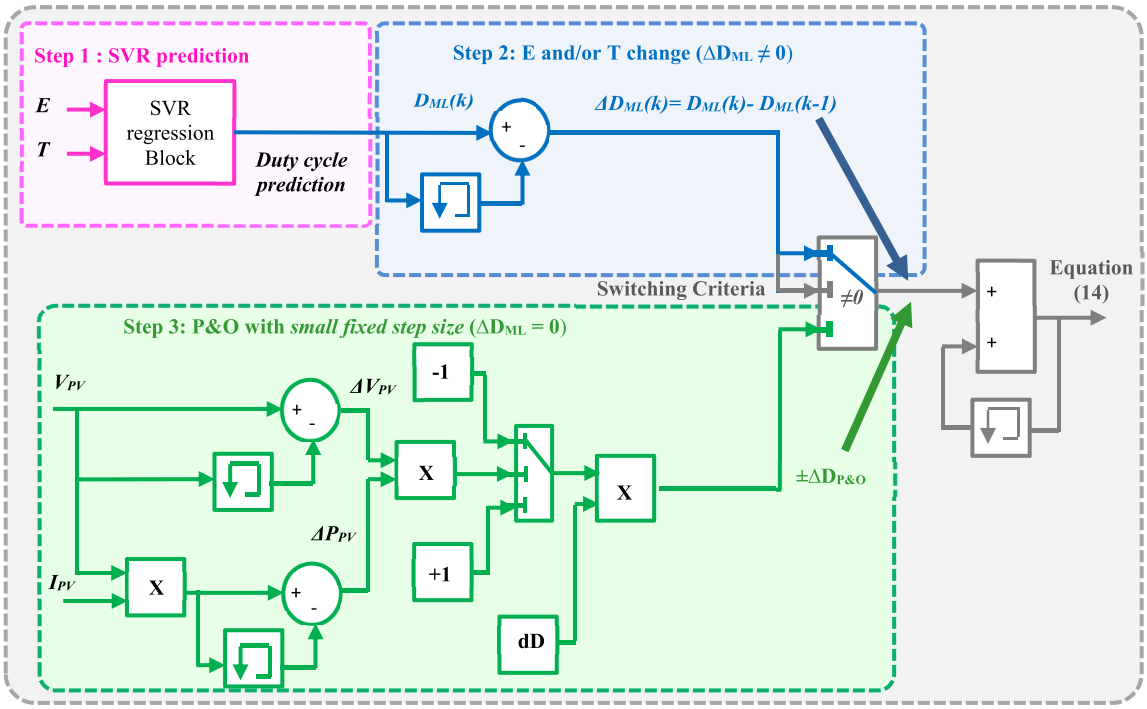

FIGURE 4. The improved SVM regression-P&O algorithm based MPPT MATLAB-Simulink model.

IV. THE DESIGN OF SVM REGRESSION-ADALINE NEURAL PQ STRATEGY

A. METHODOLOGY

The SVM regression-Adaline NPQ strategy, is a novel method of controlling the PVSAPF system. It combines Support Vector Regression based prediction approach with adaptive Adaline neural network technique, in order to improve the DC active power component extraction.

The SVM regression model is set to $T = \{(a1, b1), \ldots\ldots, (aM, bM)\}$ where aj is the input sample comprising one feature: the ignition angle of the Nonlinear load NLL ($\alpha(j)$; $j = 1 \ldots M$), and bj is output sample of SVM regression block predicting weight of Adaline ($WML(j)$, $j = 1 \ldots M$). Nine SVM regression blocks are used to predict nine weights of Adaline neural network: $WTML = [WML0, WML1, WML2, WML3, WML4, WML5, WML6, WML7, WML8]$. Figure 8 depicts the training data set collected from the simulation history of the PVSAPF system, under varying nonlinear load parameters.

Referring to Figure 9 which illustrates the proposed SVM regression-Adaline NPQ strategy for PVSAPF command, this improved hybrib algorithm can be described as follows:

After converting source voltage $V_{sa,b,c}$ and nonlinear load current $i_{NLL-a,b,c}$ into $\alpha\beta$ parameters basing on Clarke's transform, active power p and reactive power q is calculated as follows:

$$\begin{bmatrix} p \\ q \end{bmatrix} = \begin{bmatrix} v_\alpha & v_\beta \\ -v_\beta & v_\alpha \end{bmatrix} \begin{bmatrix} i_\alpha \\ i_\beta \end{bmatrix} \tag{15}$$

The instantaneous active power is also written as follows:

$$p = p_{bar} + \tilde{p} \tag{16}$$

where, p_{bar} is the DC active power component, whereas p is the fluctuating part of active power component.

In the traditional instantaneous PQ strategy, the fluctuating part of active power components extraction is ensured by the use of the Low Pass Filter (LPF). However, this extraction technique shows poor performance and a weak adaptation under a fast variation in the nonlinear load parameters [48]. Within this context, a novel hybrid harmonics extraction technique is proposed, exploiting the characteristics of intelligent learning and fast training of Adaline neural network combined with machine learning algorithms.

Consider a sinusoidal source voltage expressed by

$$V_s(t) = V_m.sin(wt + \varphi_v) \tag{17}$$

and the distorted nonlinear load current can be written as

$$i_{NLL}(t) = \sum_{h=1}^{\infty} I_h \sin(hwt + \varphi_c) \tag{18}$$

where w is the fundamental frequency, φ_c is the phase angle of current, and I_h is the amplitude of the h^{th} harmonic components. Thus, equations (17) and (18) yield to the following

$$p = p_{fund} + \begin{bmatrix} \cos(h-1)wt \\ \sin(h-1)wt \end{bmatrix}^T \begin{bmatrix} p_{n-1}\cos(\varphi_c - \varphi_v) \\ p_{n-1}\sin(\varphi_c - \varphi_v) \end{bmatrix} - \begin{bmatrix} \cos(h+1)wt \\ \sin(h+1)wt \end{bmatrix}^T \begin{bmatrix} p_{n+1}\cos(\varphi_c + \varphi_v) \\ p_{n+1}\sin(\varphi_c + \varphi_v) \end{bmatrix} \tag{19}$$

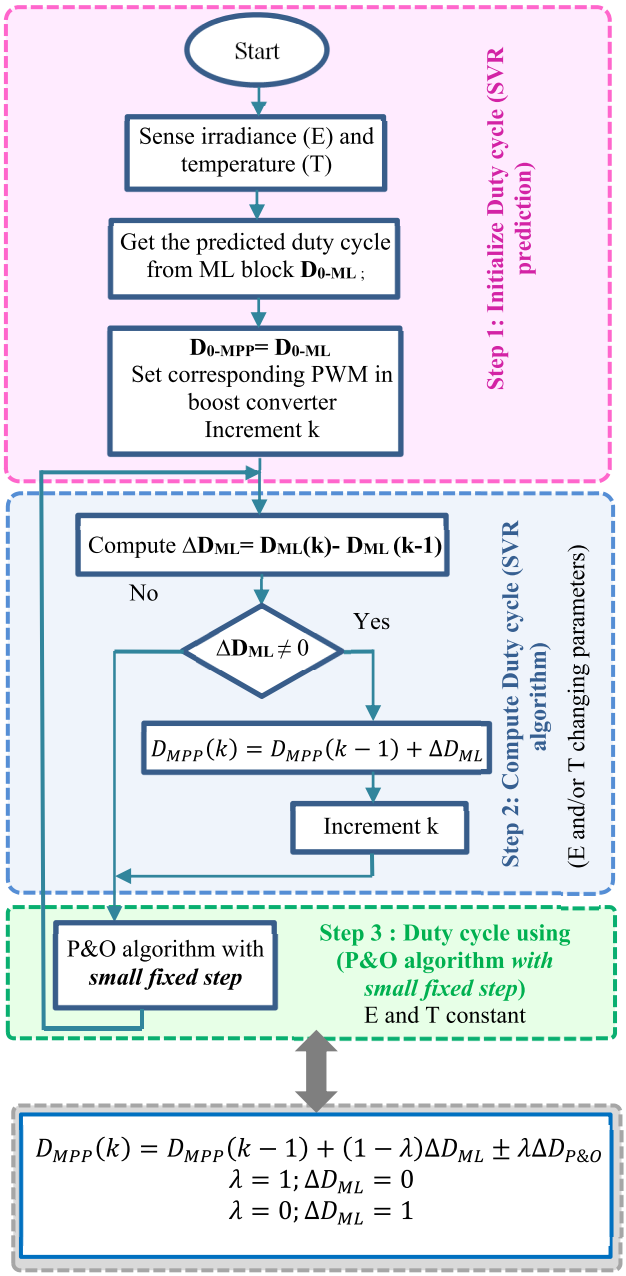

FIGURE 5. The flowchart of proposed SVM regression-P&O algorithm.

Therefore the estimated active power using ADALINE process in the matrix representation can be expressed as:

$$p_{estimated}\,(t) = W^T.X\,(t) \tag{20}$$

with the following input vector of Adaline X(t) and the weight vector of Adaline, W^T ($h = 1, 5, 7, 11 \ldots..N$)

$$X\,(t) = [1\ cos(4wt)\ \sin(4wt) \ldots \cos((h-1)\,wt)\ \sin((h-1)\,wt)\ \cos((h+1)\,wt)\ sin((h+1)\,wt)] \tag{21}$$

$$W^T = [p_{fund} \ldots p_{n-1} p_{n+1}] \tag{22}$$

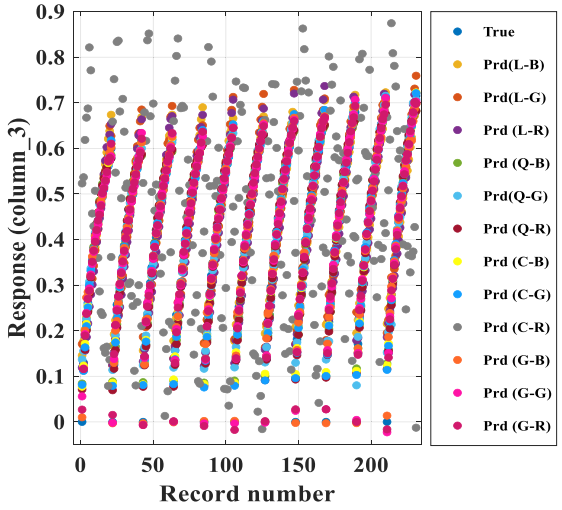

FIGURE 6. Response plot of duty cycle prediction.

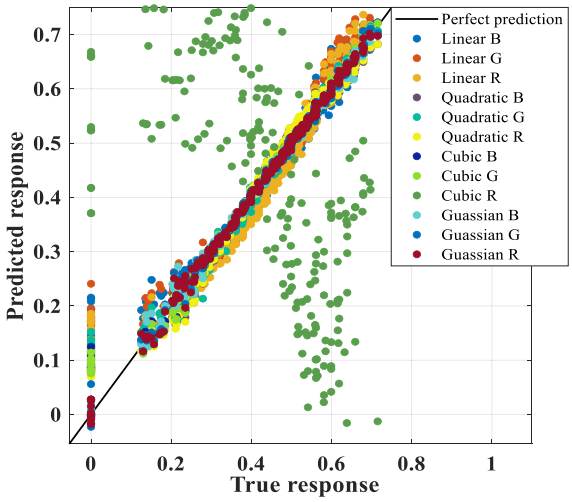

FIGURE 7. Prediction vs actual plot duty cycle prediction.

In the classical Adaline-based harmonic extraction depicted in Figure 9.a, the neural weights vector is adapted using LMS algorithm with fixed learning rate parameter μ [49],

$$W\,(k+1) = W\,(k) + \mu.e\,(k)\,.X\,(k) \tag{23}$$

where $e(k)$ is the estimation error at k time which represents the difference between the identified active power p and estimated active power $p_{estimated}$.

$$e\,(k) = p\,(k) - p_{estimated}\,(k) \tag{24}$$

After several iterations, the estimation error reaches zero and the estimated active power $p_{estimated}(k)$ becomes close to the identified active power $p\,(k)$.

However, this Adaline-based harmonics extraction technique also does not lack limitations due to the fixed learning rate parameter [50]. Several studies in the literature propose

TABLE 1. The SVM regression after training duty cycle dataset: statistics of the corresponding characteristics.

Symbol	KERNEL FUNCTION	Optimizer	RMSE	R-squared	MSE	MAE
L-B	Linear	Bayesian optimization	0,047558	0,93	0,0022617	0,028274
L-G	Linear	Grid search	0,047224	0,93	0,0022301	0,029055
L-R	Linear	Random search	0,045345	0,93	0,0020562	0,033893
G-B	Gaussian	Bayesian optimization	0,011365	1	0,00012915	0,0079605
G-G	Gaussian	Grid search	0,010425	1	0,00010869	0,0072496
G-R	**Gaussian**	**Random search**	**0,0094678**	**1**	**0,0000896**	**0,0067274**
Q-B	Quadratic	Bayesian optimization	0,027225	0,98	0,00074122	0,018141
Q-G	Quadratic	Grid search	0,03095	0,97	0,00095791	0,017173
Q-R	Quadratic	Random search	0,026902	0,98	0,0007237	0,019318
C-B	Cubic	Bayesian optimization	0,023356	0,98	0,00054552	0,011015
C-G	Cubic	Grid search	0,022268	0,98	0,00049588	0,011509
C-R	Cubic	Random search	0,36605	-3,44	0,13399	0,32422

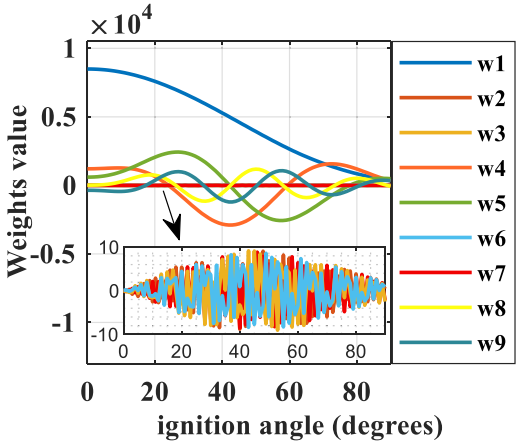

FIGURE 8. Weighs waveform under varying ignition angle of NLL (Dataset).

an adaptive learning rate parameter [51], while others propose various techniques for learning rate optimization [52].

In this work, a new weights updating technique is proposed and detailed in Figure 9.b. The idea is to use the SVM regression algorithm for predicting the initials weights (blue line) to get the estimated active power $p_{estimated}$ close to the identified active power p, thus, reducing speedily the estimation error. The process is then switched to the LMS algorithm (red line) using a small learning rate parameter for accurate convergence.

The flowchart of the proposed hybrid harmonics extraction approach is depicted in Figure 10, detailing the different steps of the updating weights and the training algorithm. The proposed weights updating expression is as follow:

$$\begin{cases} W(k+1) = (1-\Psi).W_{ML} \\ \qquad +\Psi\,(W(k) + \mu.e(k).X(k)) \\ \Delta\alpha = 0 \rightarrow \Psi = 1 \\ \Delta\alpha \neq 0 \rightarrow \Psi = 0 \end{cases} \tag{25}$$

where ψ is switching function $\psi \in \{0, 1\}$, $\Delta\alpha$ is the difference between the current ignition angle of the nonlinear load NLL α (k) and the last one $\alpha(k\text{-}1)$, and W_{ML} the predicted weights vector of Adaline expressed as follows:

$$W^T_{ML-initiation} = \left[p_{bar-init} \cdots p_{N-1,init} p_{N+1,init}\right] \tag{26}$$

Finally, after extracting the DC active power component the reference currents are determined as follows:

$$\begin{bmatrix} i_{NL-\alpha} \\ i_{NL-\beta} \end{bmatrix} = \frac{1}{V^2_{grid-\alpha} + V^2_{grid-\beta}} \begin{bmatrix} V_{grid-\alpha} & -V_{grid-\beta} \\ V_{grid-\beta} & V_{grid-\alpha} \end{bmatrix} \times \begin{bmatrix} -p_{ref} \\ -q_{ref} \end{bmatrix} \tag{27}$$

$$\begin{bmatrix} i_{ref-Fa} \\ i_{ref-Fb} \\ i_{ref-Fc} \end{bmatrix} = \sqrt{\frac{2}{3}} \begin{bmatrix} 1 & 0 \\ -\frac{1}{2} & \frac{\sqrt{3}}{2} \\ -\frac{1}{2} & -\frac{\sqrt{3}}{2} \end{bmatrix} \begin{bmatrix} i_{NL-\alpha} \\ i_{NL-\beta} \end{bmatrix} \tag{28}$$

B. SVM REGRESSION-BASED WEIGHTS VECTOR PREDICTION

In order to select the best kernel function and Hyperparameter optimization method of the nine SVM regression blocks, the SVM regression model of each weight is trained, and then evaluated. The training results for the first weight W_{ML0} are grouped and presented by: the predicted response versus record number and the predicted versus actual plot as shown in Figure 11 and Figure 12 respectively.

Therefore, based on the comprehensive performance comparison of W_{ML0} summarized in Table 2, the Cubic kernel function with Grid search Hyperparameter optimization method (C-G) is selected and used in SVM regression algorithm for best W_{ML0} prediction.

The same method of selection is applied to the remaining predicted weights models. Figure 13 and Figure 14 display MSE and MAE under various Kernel function-Optimizer for the nine weights models of prediction, respectively.

Finally, the overall results of the best kenel function and Hyperparameter optimization method for each SVM regression block is presented in Table 3.

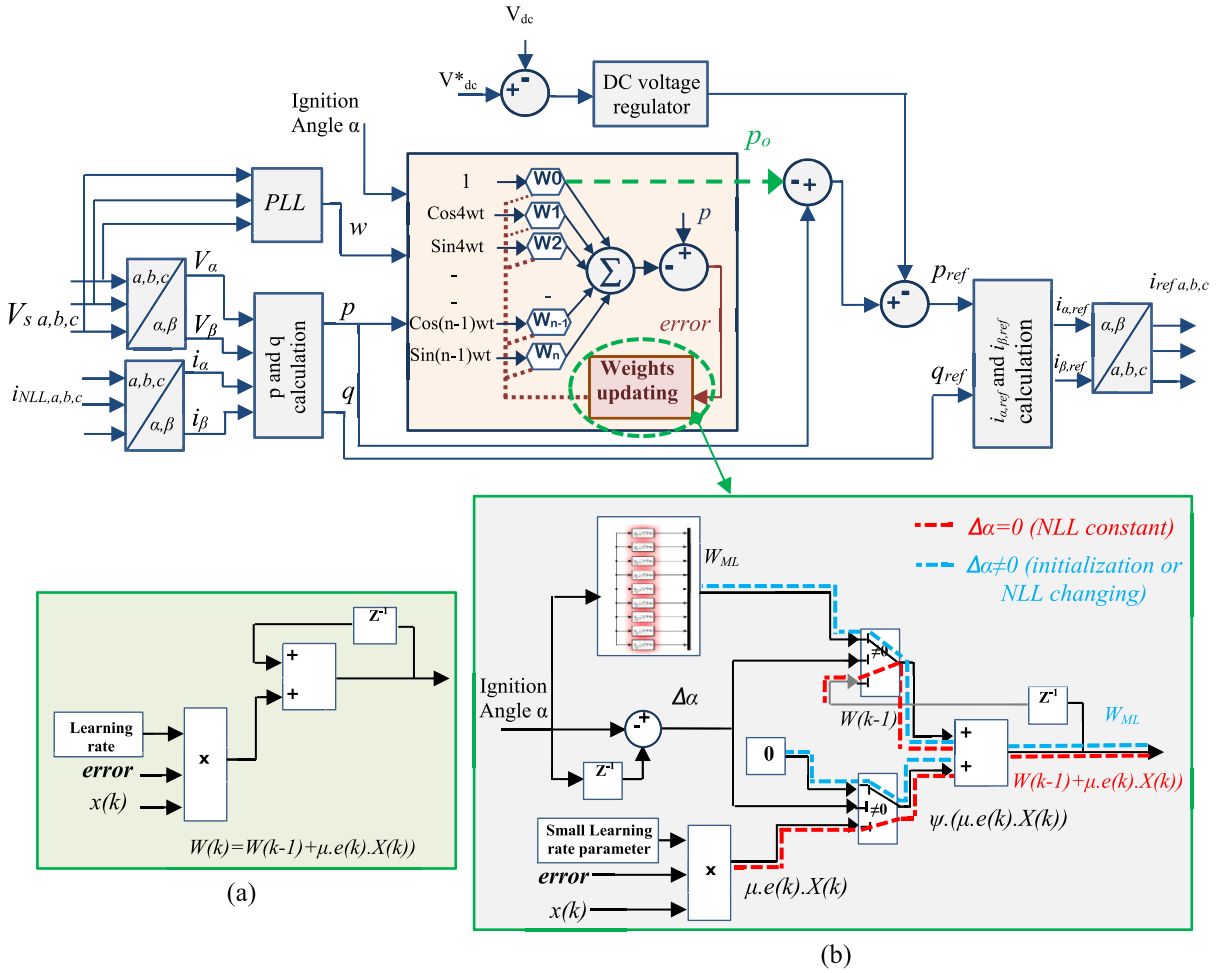

FIGURE 9. The proposed SVM regression-Adaline neural PQ strategy for PVSAPF command. (a): The classical weights updating technique (b): The proposed new weights updating technique.

V. ANALYSES AND VALIDATION

In this section, in order to assess the advantages of the suggested Machine Learning based approaches for maximum power point tracking and harmonics detection, a comprehensive simulation of the whole PVSAPF system, exhibited in Figure 1, has been performed in MATLAB/Simulink environment. Hence, a comparative study is given for each novel strategy with other existing ones, under a sudden change of NLL parameters and/or climate conditions.

The whole characteristics and the stability proof of the proposed machine learning based methods are given in Table 4 and the Appendix, respectively.

A. SVM REGRESSION-P&O APPROACH PERFORMANCE ASSESSMENT

1) SVM REGRESSION-P&O APPROACH BASED DUTY CYCLE CONVERGENCE

Duty cycle D and ΔD duty cycle variation of the proposed SVM regression-P&O based MPPT strategy under different simulation cases is displayed in Figure 15.

First the duty cycle is initialized by the predicted output of SVM regression block ($D_0 = D_{0-ML} = 0.56$) then the algorithm switches to P&O algorithm (a) using a small fixed step $\Delta D_{P\&O} = 0.0001$.

At $t = 0.5s$, the temperature changes from $15°$ to $33°$, therefore the algorithm switches back to the SVM regression model in order to generate a new predicted output.

ΔDML which represents the difference between the current predicted SVM output and the last one is equal to 0.04 (orange line at 0.5s) and is added to the last duty cycle D (k-1) to formulate the new one $D\ (k) = D\ (k\text{-}1) + \Delta DML = 0.562+0.038 = 0.6$. The algorithm switches again to P&O algorithm with $\Delta\ D_{P\&O} = 0.0001$ to track accurately this novel MPP corresponding to ($33°$ and $810W/m^2$): $D\ (k+1) = D\ (k) \pm \Delta DP\&O$.

This hybrid algorithm is reproduced again when the irradiance varies (from $810W/m^2$ to $450W/m^2$; at $t = 0.1s$): $\Delta DML = -0.18$ is added to the last duty cycle of the last MPP (b) to obtain $D(k) = D(k\text{-}1) + \Delta DML = 0.62\text{-}0.18 = 0.42$ which will be closed to the novel MPP.

TABLE 2. The SVM regression after training duty cycle dataset: statistics of the corresponding characteristics.

	Optimizer		R-squared	MSE	MAE
Linear	Bayesian optimization	332,67	0,99	1,1067E+05	271,47
Linear	Grid search	330,86	0,99	1,0947E+05	269,72
Linear	Random search	321,52	0,99	1,0338E+05	276,35
Gaussian	Bayesian optimization	194,96	1	3,8101E+05	81,68
Gaussian	Grid search	179,03	1	3,2051E+04	50,312
Gaussian	Random search	726,72	0,93	5,2813E+05	514,64
Quadratic	Bayesian optimization	334,5	0,99	1,1189E+05	281,42
Quadratic	Grid search	324,07	0,99	1,0502E+05	288,81
Quadratic	Random search	333,69	0,99	1,1130E+05	294,55
Cubic	Bayesian optimization	63,708	1	4,0587E+03	56,994
Cubic	**Grid search**	**33,054**	**1**	**1,0926E+03**	**25,55**
Cubic	Random search	33,695	1	1,1354E+03	21,873

TABLE 3. The SVM regression after training all the weight of adaline DATASET: results of the best kenel function and Hyperparameter statistics of the corresponding characteristics.

Symbol	KERNEL FUNCTION	Optimizer	RMSE	R-squared	MSE	MAE
W1	Cubic	Grid search	33,054	1	1,0926E+03	25,55
W2	Gaussian	Grid search	4,3857	0	1,9234E+01	3,5969
W3	Linear	Grid search	4,6802	0,01	2,1905E+01	3,863
W4	Gaussian	Grid search	9,221	1	8,5028E+01	4,0929
W5	Gaussian	Grid search	4,0587	1	1,6473E+01	3,1091
W6	Quadratic	Random search	4,3243	0,03	1,8699E+01	3,5283
W7	Gaussian	Random search	4,3888	0,01	1,9262E+01	3,6493
W8	Gaussian	Grid search	3,1438	1	9,8834E+00	2,4451
W9	Gaussian	Grid search	5,6303	1	3,1700E+01	3,1027

TABLE 4. Proposed ML-based algorithm characteristics.

Proposed strategy	Dataset ,Fields and Features
The SVM-P&O MPPT algorithm	• **Dataset :** TMPP={(x1,y1),……., (xn, yn)}. xj is the input sample comprising two features : • The irradiance E (from 0W/m* to 1000W/m²). • The temperature T (from 0° to 50°). yj is output sample of SVM regression block comprising one feature : • The duty cycle DML(j) of the boost converter (The dataset size is 231).
The SVM Regression-Adaline Neural PQ strategy	• **Dataset :** T= {(a1,b1),……., (aM, bM)} Nine SVM regression blocks are used to predict nine weights of Adaline neural network: WTML= [WML0, WML1, WML2, WML3, WML4, WML5, WML6, WML7, WML8]. aj is the input sample comprising one feature: • The ignition angle of the Nonlinear load NLL (α(j); j=1…M) : From 0° to 90°. bj is the output sample comprising one feature : • The weight of Adaline (WML(j), j=1…M). From WML(1) to WML(91).

P&O algorithm with a small fixed step is then started again and continues until the corresponding duty cycle of MPP is followed: $D(k+1) = D(k) \pm \Delta DP\&O = 0.426$.

As a result, it can be concluded that:

- The use of SVM regression block, which predicts an initial duty cycle, allows P&O algorithm to work with a small fixed step.

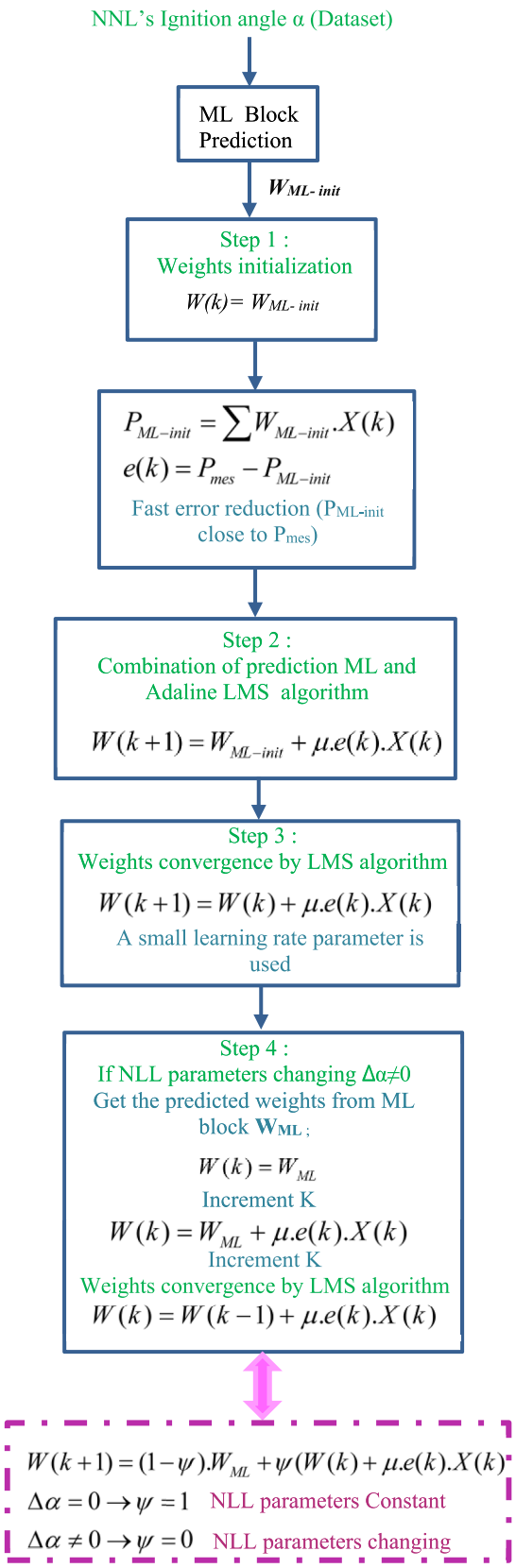

FIGURE 10. The flowchart of the proposed hybrid harmonics extraction approach.

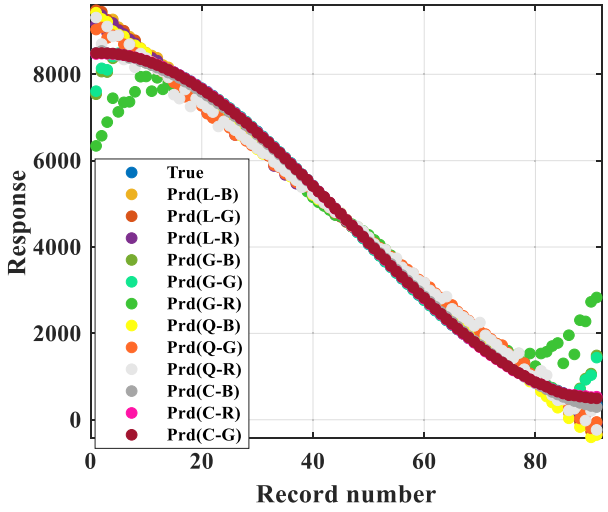

FIGURE 11. Response plot SVR_W1.

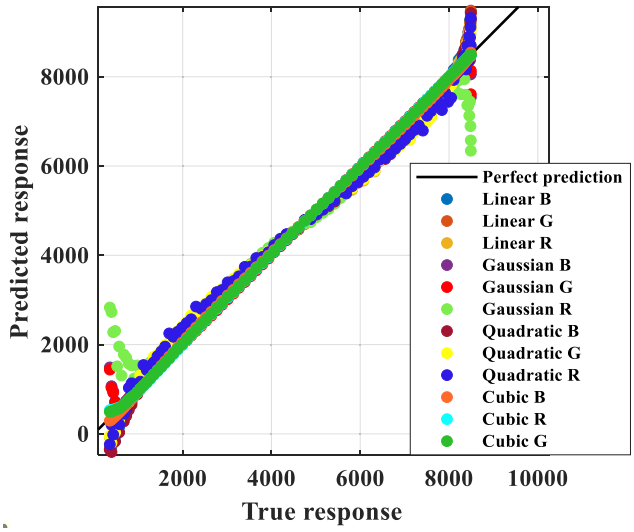

FIGURE 12. Prediction vs actual Plot SVR_W1.

- The use of P&O algorithm, which finalizes the pursuit of the MPP, allows to the SVM block to work with a medium dataset (a very precise prediction of duty cycle is not required), i.e., with moderate computational load.

In the next simulation cases, the proposed SVM regression-P&O MPPT controller is compared to the Fuzzy logic MPPT controller (developed in previous study [58]), and to the classical P&O strategy in terms of:

- PV energy losses.
- Performance tracking and adaptation ability to temperature and/or irradiance variations.

2) SVM REGRESSION-P&O APPROACH UNDER G AND/OR T CHANGING

Duty cycle variation and the corresponding maximum PV power *Pmp*, under variable temperature and variable

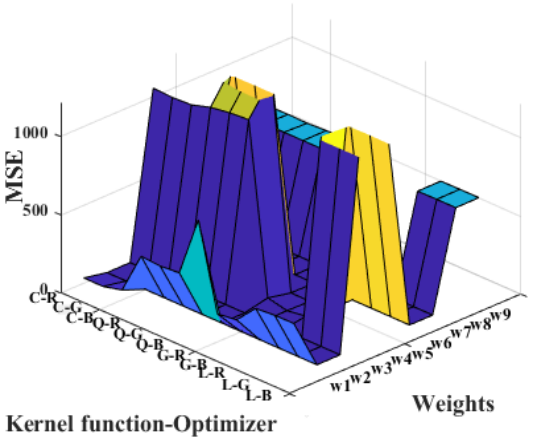

FIGURE 13. Prediction MSE under various Kernel function-Optimizer for different weights of Adaline.

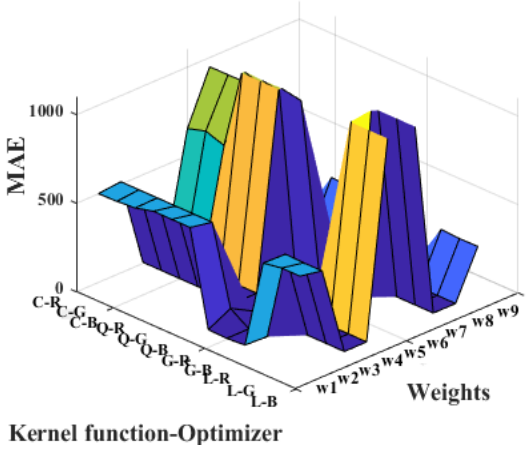

FIGURE 14. Prediction MAE under various Kernel function-Optimizer for different weights of Adaline.

irradiance are depicted in Figure 16. As it can be noticed, the proposed machine learning-based MPPT strategy has a very fast response time compared the other used algorithms. Indeed, as shown in Figure 17, the Duty cycle converges in an average of 1ms by SVR regression P&O strategy against 100ms and 50ms by the classical P&O algorithm and the fuzzy MPPT controller, respectively.

In addition, this fast convergence of duty cycle leads to a speed maximum power point MPP tracking, which implies a systematic reduction in PV energy losses. As expected, Figure 18 and Figure 19 indicate 99% of PV energy decrease by the proposed by SVR regression P&O strategy compared to the classical P&O MPPT strategy showing a successful exploitation of PV panel power.

In order to rate the dynamic response of SVM regression P&O strategy behavior compared to the above mentioned MPPT strategies, the system is subjected simultaneously to both a sudden variable temperature changes (45, 15, 5 and 35 degrees (Figure 20.a)) along with an abrupt insolation parameters (800,600,150 and 500 W/m^2(Figure 20.b)).

TABLE 5. The new SVM regression P&O strategy performance tracking.

MPPT Algorithm	(A) D%	(A) tr(s)	(B) D%	(B) tr(s)	(C) D%	(C) tr(s)
P&O	8,3%	0.03s	3,41%	0.029s	3.26%	0.025s
FLC	7,9%	0.03s	2.9%	0.029s	2.43%	0.025s
SVM regression-P&O	**0,46%**	**0.02s**	**0.01%**	**0.02s**	**0.55%**	**0.01s**

The maximum solar current *Imp*, the maximum solar voltage *Vmp*, and the PV active power *Pmp* variation is depicted in Figure 20.c, Figure 20.d, and Figure 20.e, respectively. The zoomed waveforms indicate that the novel SVR regression P&O strategy shows a strong adaptation with respect to the change of the operating point of the solar panel.

The dynamic performance of the proposed SVM regression P&O, the intelligent Fuzzy Logic and the classical P&O controllers are summarized in Table 5. The analysis of results shows that the percentage of decrease in overshoot and response time; by using the proposed method; reaches up to 94.84% and 60%, respectively.

Furthermore, a literature survey is presented in Table 6, which reviews recent publications on various MPPT strategies using machine learning. It involves various criteria along with a brief comparative assessment relating to the uniqueness of the proposed SVM-regression P&O strategy.

B. SVM REGRESSION-ADALINE NEURAL PQ STRATEGY APPROACH PERFORMANCE ANALYSES

In this second part, various simulation scenarios were addressed in order to evaluate the performance and the superiority of this second proposed technique, i.e SVM regression-Adaline NPQ strategy, for harmonics extraction speed convergence, accuracy and adaptation ability to sudden nonlinear load variation. Within this context, the PQ technique of control, using Machine Learning block combined with ADALINE network is compared to that based on ADALINE network, and then to that using the low pass filter LPF.

Figure 21 displays the results of updating the nine weights waveforms (*W1* to *W9*) under a variable nonlinear load parameter (30°, 80°, 60° and 5°) using both Machine

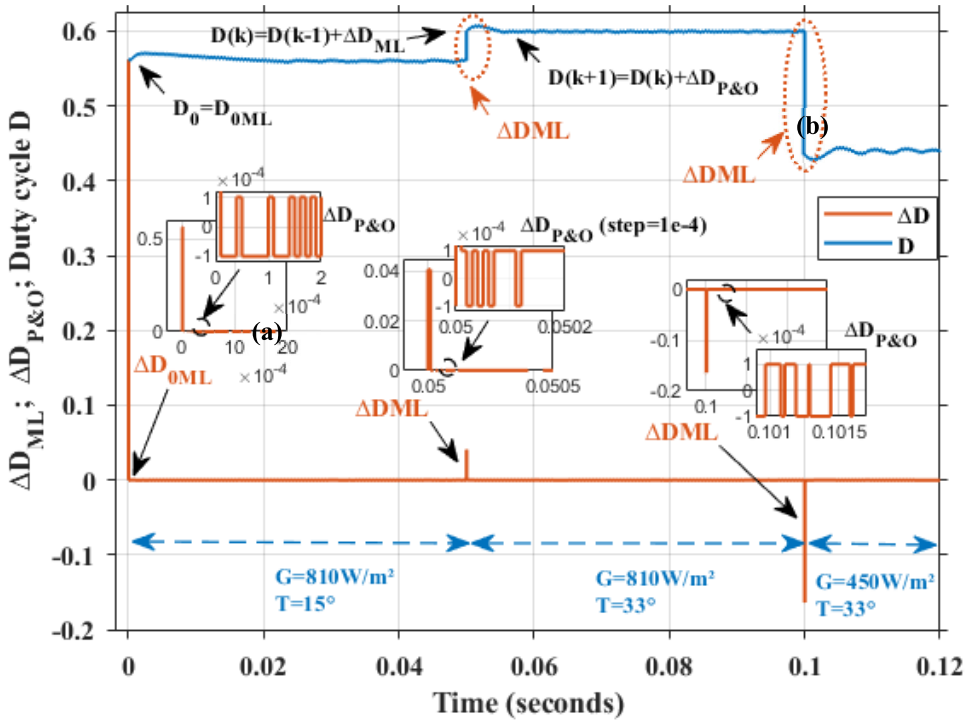

FIGURE 15. The Duty cycle D and ΔD duty cycle variation of the proposed SVM regression-P&O based MPPT strategy.

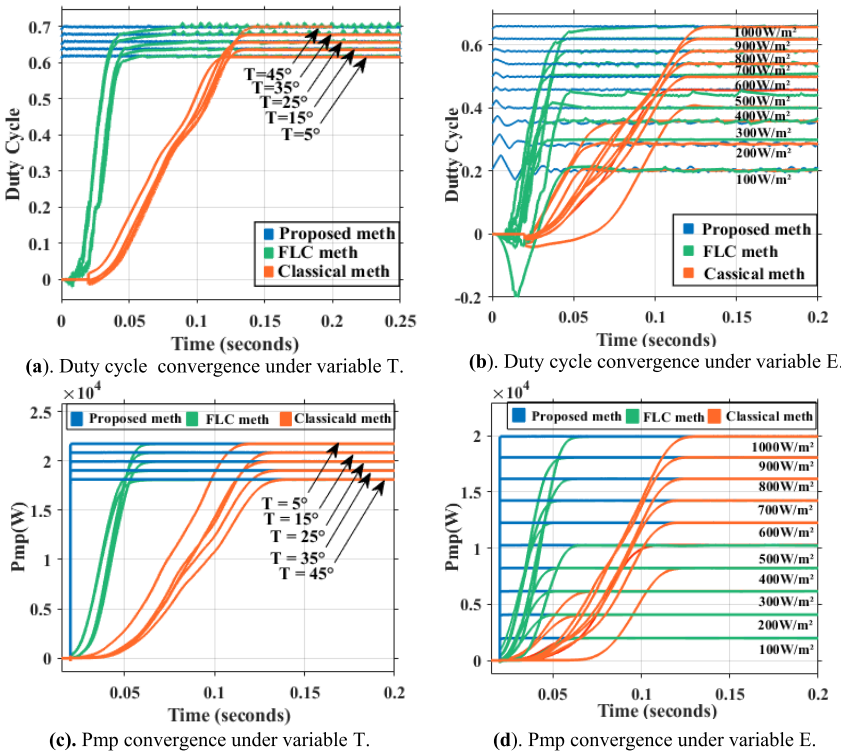

(a). Duty cycle convergence under variable T.

(b). Duty cycle convergence under variable E.

(c). Pmp convergence under variable T.

(d). Pmp convergence under variable E.

FIGURE 16. Duty cycle variation and the corresponding maximum PV power Pmp, under variable temperature and variable irradiance.

Learning based Adaline Neural-PQ strategy (marked 'ML-ANN') and the conventional Adaline Neural-PQ technique (marked 'ANN').

As expected, the proposed novel strategy gives an excellent waveforms quality in terms of speed convergence, overshoot and accuracy. In fact:

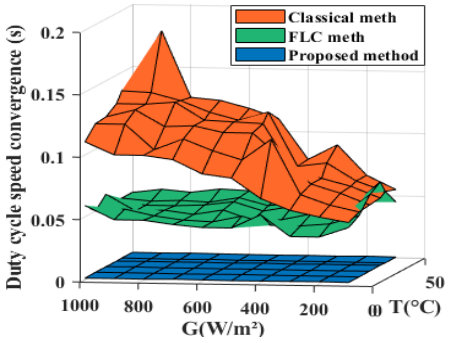

FIGURE 17. Duty cycle speed convergence under variable irradiance and temperature.

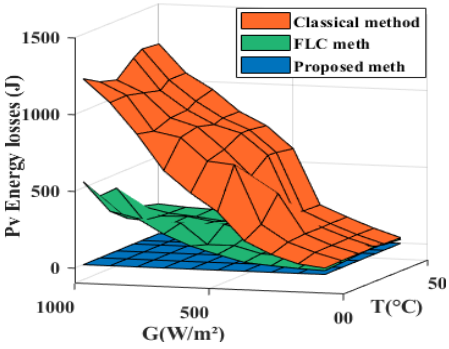

FIGURE 18. PV energy losses under different MPPT strategy.

- The nine SVM regression blocks output generate the predicted initials weights (*W1ML,…, W9ML*) to get an initial DC active power component close to the identified one.
- As depicted in Figure 22, the weights waveform does not present any overshoot, whereas in the weights curve obtained by the classical neural method the overshoot peaks reach up to 386.451%.
- The estimation error is then reduced speedily as it can be noticed in Figure 23 and Figure 24 (the initial error obtained by the proposed strategy is lower up to 88% than that obtained by the classical Adaline Neural-PQ technique).
- After predicting initials weights by SVM regression blocks, the process is then switched to LMS based Neural algorithm with a small well as less oscillation than the classical Adaline based extraction strategy.

Figure 25 and Figure 26 present a comparative study of the DC active power component extraction under a fixed (30°) and variable nonlinear load parameter (30°, 80°, 60° and 5°), respectively, using the proposed hybrid strategy with a small learning rate parameter μ = 15e-4 (marked 'ML'), and the classical Adaline neural based technique; (marked 'ANN'); using first the same learning rate parameter μ = 15e-4 and then a large one μ = 15e-3.

TABLE 6. Literature Review of previous similar works.

Ref	ML method	Description	Dataset	MSE	RMSE	MAE	Response Time	Comparative Assessment
[53]	LSTM-DL	E and T are the inputs and Vmp is the target of LSTM network. The controlled output voltage of the PV array is compared to the actual PV voltage, and error is minimized using PI control.	1 million data points	0.4	0.2	0.0016	-	Efficient for uncertain (need large datasets) Overcome challenges of RNN by adding LSTM cell with less complexity.
[54]	ANN ANN-P&O	E and T are used as inputs to the neural network. The number of layers is determined by the hit-and-trial method. The duty ratio for the converter is the output. In this control method, the neural network output is combined with the output and the average of the duty ratio generated is given to the PWM generator for generating switching pulses.	1000 data points T (15° to 35°) E (0 to 1000 W/m2).	- -	2.3e-11 at 1000 epoch	- -	0.05s 0.005s	Accuracy is improved for better performance. Big dataset. High Computational time. This method helps in reducing the cost of the system by reducing the number of sensors.
[55]	HC-ANN	This method Combines conventional hill climbing (HC) algorithm and artificial neural networks (ANN). Two-stage global maximum power point tracking (GMPPT) method is designed.	4000 input-output training data pairs	0.289	-	-	0.019 s	Does not require irradiance or temperature sensors. Large datasets.

As it can be noticed, in the classical Adaline based Neural strategy, the tracking speed of the DC active power component extraction is improved by using a large learning rate value (μ = 15e-3) but with the penalty of providing fluctuations in the steady state. However, the use of a small learning rate parameter (μ = 15e-4) improves stability but slows up the response time of the DC active power component extraction. Therefore, as it can be seen in the zoomed waveforms in Figure 25 and Figure 26, the proposed SVM regression-Adaline based harmonic extraction technique demonstrates its supremacy compared to the classical Adaline based Neural strategy and to the conventional one

TABLE 6. *(Continued.)* Literature Review of previous similar works.

Ref	ML method	Description	Dataset	MSE	RMSE	MAE	Response Time	Comparative Assessment
[56]	LSTM model based MPPT	The neural network estimates the output resistance of the PV module by using the input parameters temperature and irradiation.	5511 data points	0.0159	0.1261	0.079	-	The LSTM model could follow Rpv with the mean absolute error value of 95.2 Ω.
	Linear regression based MPPT	Temperature and irradiation parameters were used as the independent variables and the output resistance of the PV module was used as the dependent variable.	-	0.3226	0,5979	0.4721	-	The linear regression model could predict Rpv with the mean absolute error value of 566,6Ω.
[57]	SVM-P&O	The perturbation step size is determined offline for a specific location based on the local irradiance data. The SVM is employed to automatically classify the desert or coastal locations using historical irradiance data. The perturbation step size is optimized for better system performance without increasing the control complexity.	197 samples of coastal area and 22 samples of desert area	-	-	-	tracking efficiency is 99.92%, compared to the classical adaptive MPPT	-The performances are highly dependent on the chosen step size. -The step-size also can be updated monthly or seasonally for better system performance without increasing the control complexity.
Our study	SVM REGRESSION-P&O	-Four kernel functions with three Hyperparameter optimization methods are tested in order to get the best duty cycle prediction by SVM regression model. -The SVM regression block predicts an initial duty cycle according to irradiance E and T. - The process is then switched to P&O algorithm using a small fixed step in order to accurately track the MPP. -The algorithm adapts perfectly to the changing parameters of the solar panel.	231 data T (0° to 50°) E (0 to 1000 W/m2).	0,000089	0,0094	0,0067	0.001s	-The SVM block output ensures high tracking speed performance. -The combination of the SVM block (which predicts the initial duty cycle) with a small step P&O, ensures high MPPT performance without requiring a variable step generation (unlike the variable-step ML methods where the performances are highly dependent on the chosen step size). - High accuracy in the initial duty cycle value predicted by the SVM block is not recommended. The duty cycle precision is provided by a small step P&O. The computational load is lower.

using LPF. Indeed, it gives a significant fast convergence (thanks to the output prediction of SVR regression block), and accurate steady state response (thanks to the used small learning rate parameter).

C. PV-SAPF SYSTEM PERFORMANCES USING ML_SVR-MPPT WITH ML_SVR ADALINE EXTRACTION

1) GRID POWER TRANSIT AND DC VOLTAGE REGULATION

The third part focuses on the grid power transit and DC voltage regulation of the PVSAPF system. The whole studied system is simulated under varying nonlinear Load NLL parameters (from 0s to 0.6s), then under solar variation (from 0.6s to 1s).

The Grid power PG waveform under different harmonics detection strategies is depicted in Figure 27: the proposed SVM regression-Adaline neural PQ method of control (marked 'ML-adaline'), the intelligent adaptive Adaline neural PQ strategy (marked 'Adaline') and the classical PQ strategy using LPF (marked 'LPF'). P&O algorithm is used for MPPT controller in all the simulation cases of Figure 28. Table 4 gives the summary of dynamic performance of the controlled PVSAPF system.

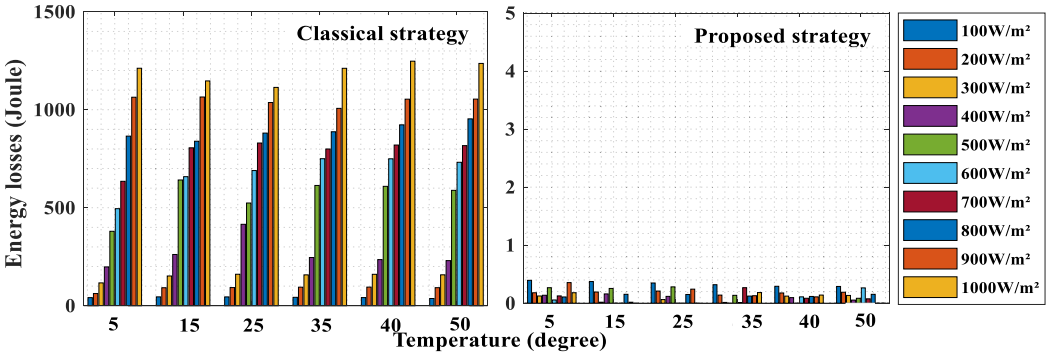

FIGURE 19. PV Energy losses distribution by the classical P&O algorithm and the proposed SVR regression-P&O strategy.

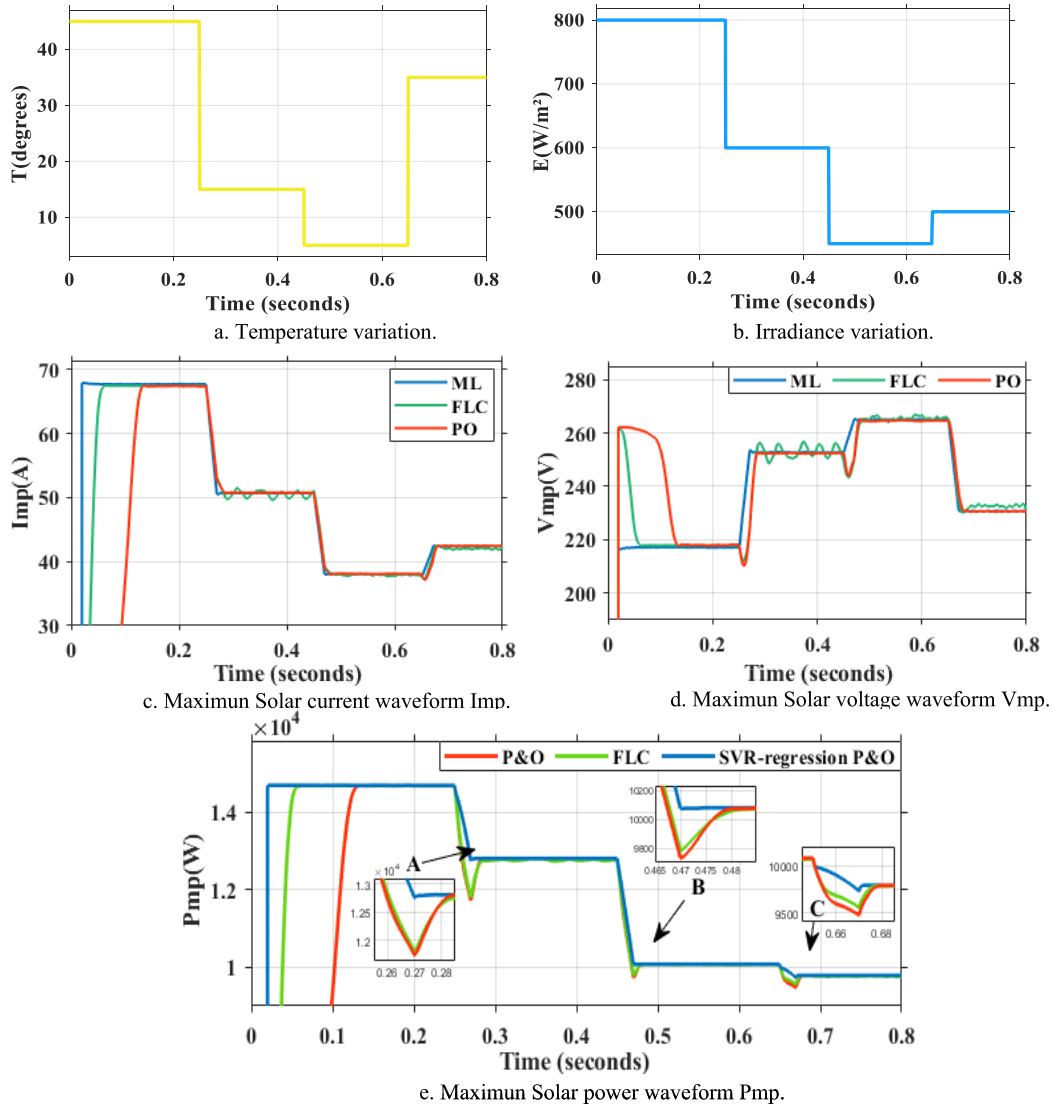

a. Temperature variation.
b. Irradiance variation.
c. Maximun Solar current waveform Imp.
d. Maximun Solar voltage waveform Vmp.
e. Maximun Solar power waveform Pmp.

FIGURE 20. Dynamic response of SVM regression P&O strategy behavior under G and T changing.

It can be observed that during NLL variation (from 0s to 0.6s), the response is faster in the case of the new SVM regression-Adaline neural PQ strategy and it also shows less overshoot than the other compensation methods. However, during irradiance variation (from 0.6s to 1s), similar dynamic performances have been exhibited for all the

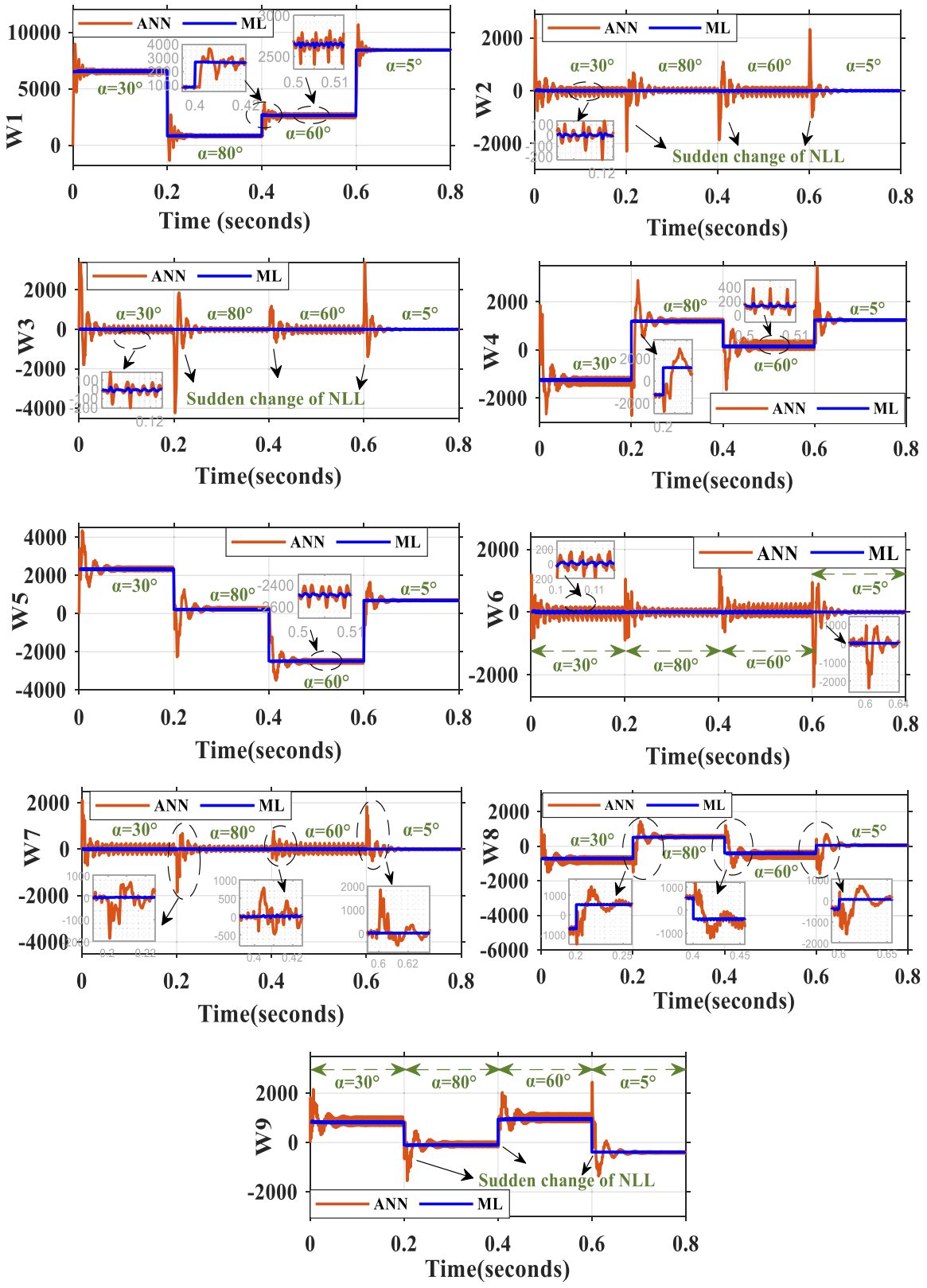

FIGURE 21. The nine updating weights waveforms (W1 to W9) under abrupt variation of the nonlinear load parameter (30°, 80°, 60°and 5°).

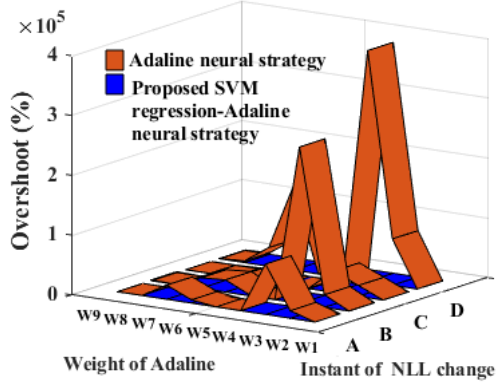

FIGURE 22. Overshoot of the nine weights of Adaline under NNL variation.

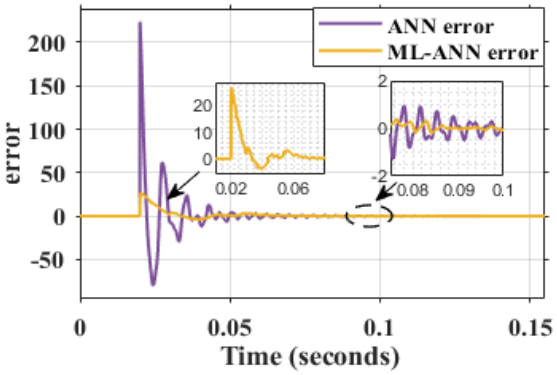

FIGURE 23. The estimation error waveform under a fixed nonlinear load parameter (α =30°).

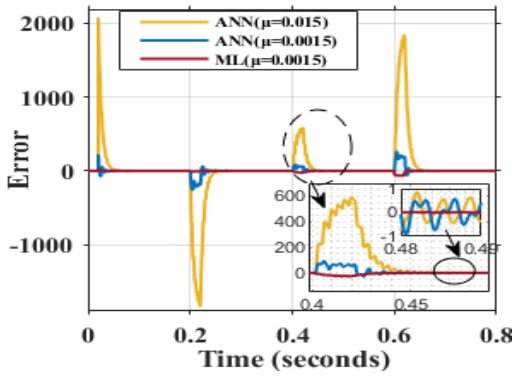

FIGURE 24. The estimation error waveform under variation of the nonlinear load parameter (30°, 80°, 60° and 5°).

compensating strategies of PV SAPF system. It is understood that:

- the compensation methods act on the dynamic performance of the PV SAPF during the variation of the NLL load.
- the proposed SVM regression-Adaline neural PQ strategy is found to be the most appropriate during the sudden variation of the operating point of the nonlinear load.

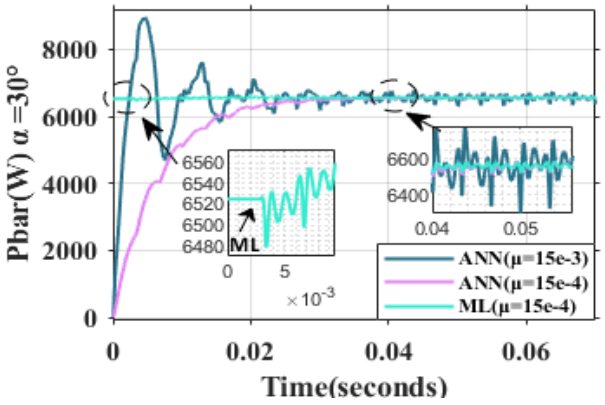

FIGURE 25. The DC active power component extraction waveform under a fixed NLL (30°).

The variation of the Grid power PG under different MPPT strategies is depicted in Figure 28. The SVM regression-Adaline neural PQ is selected as compensating strategy of the studied PVSAPF system, whereas, different simulation cases have been performed under various MPPT controllers, namely, the novel SVM regression-P&O strategy (marked 'ML-P&O'), Fuzzy logic MPPT (marked 'FLC') and the classical P&O algorithm (marked 'P&O'). From the zoomed curves and the data presented in Table 7, the novel SVM regression-P&O during irradiance variation (from 0.6s to 0.8s) presents the better dynamic performance in terms of overshoot and response time than the other MPPT strategies, while during NLL variation (from 0s to 0.6s) similar dynamic performances have been showed for all simulations cases of PV SAPF system. It can be concluded that MPPT methods act on the dynamic performance of the PV SAPF during the variation of PV- insolation, and the proposed SVM regression-P&O strategy is the most appropriate during a sudden variation of the operating point of the PV panel.

In the last scenario, the PVSAPF system dynamic performances are evaluated in Figure 29 and Figure 30 using the proposed method of control, i.e, the new SVM regression-P&O strategy for MPPT combined with the new SVM regression-Adaline neural PQ method of control. It can be noticed that the DC link voltage waveform maintains perfectly its reference under a sudden variation on PVSAPF system parameters.

In addition, the results summarized in Table 7 and presented in Figure 31 and Figure 32 clearly demonstrate that this proposed machine learning based-combination presents lower overshoot and fast response time than the classical one whatever the change of NLL parameters and irradiance levels.

2) PV INTEGRATED WITH SHUNT ACTIVE POWER FILTER PERFORMANCE ANALYSES

In order to investigate all operating modes of the ML-based integrated PV shunt active power filter, various simulation scenarios are examined at different functioning points of the system, as shown in Figure 33.a.

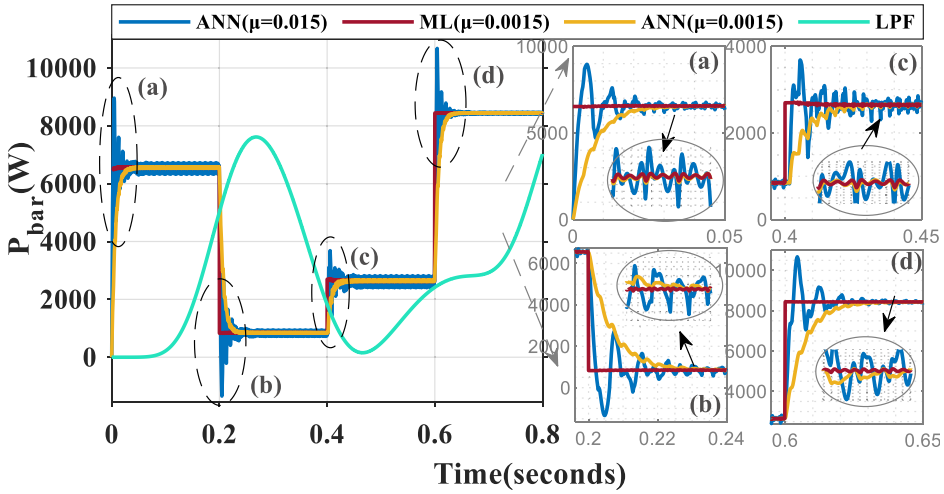

FIGURE 26. The DC active power component extraction waveform under variation of the nonlinear load parameter (30°, 80°, 60°and 5°).

TABLE 7. PVSAPF performance tracking with The proposed ML-SVR-P&O for MPPT combined with the proposed ML-Adaline strategy for harmonics extraction.

Figure	MPPT Algorithm	Harmonic Extraction strategy	(A) D%	(A) tr(s)	(B) D%	(B) tr(s)	(C) D%	(C) tr(s)
	P&O	LPF	2.89%	0.09s	11.63%	0.08s	56%	0.083s
Figure 28	P&O	Adaline	1.31%	0.05s	2.58%	0.046s	56%	0.083s
	P&O	ML-Adaline	**0.24%**	**0.04s**	**0.45%**	**0.02s**	56%	0.083s
	P&O	ML-Adaline	0.02%	0.023s	0.1%	0.02s	59.6%	0.13s
Figure 29	FLC	ML-Adaline	0.02%	0.024s	0.1%	0.02s	59.6%	0.058s
	ML-SVR-P&O	ML-Adaline	0.02%	0.023s	0.1%	0.02s	**10.5%**	**0.03s**
Figure 30	P&O	LPF	1.68%	0.077s	6.6%	0.047s	92.3%	0.093s
	ML-SVR-P&O	ML-Adaline	**0.08%**	**0.02s**	**0.06%**	**0.024s**	**10%**	**0.03s**
Figure 31	P&O	LPF	0.29%	0.074s	0.76%	0.09s	2.33%	0.078s
	ML-SVR-P&O	ML-Adaline	**0.02%**	**0.012s**	**0.005%**	**0.007s**	**0.87%**	**0.076s**

TABLE 8. THD performance under solar and load variations.

E(W/m²), α(°)	Total Harmonic Distortion (%)			
	Classical strategy (P&O, PQ)	FLC-based strategy	Adaline_based Strategy	Proposed ML-based strategy
200W/m²,0°	4.79	4.66	4.7	**4.48**
600 W/m²,90°	2.92	2.72	2.6	**2.45**
0 W/m²,0°	2.71	2.63	2.6	**2.54**

The active power transit shown in Figure 33.b exactly matches the power transit analysis discussed previously in Part II.A. Indeed:

- From 0s to 0.3s, as Ppv = 0W (E = 0W/m^2), the AC grid delivers the entire requested power to the nonlinear load (Ppv = 0W; $P_G = P_L$).
- From 0.3 s to 0.6 s, the irradiation level increases from 0 to 200 W/m2. The solar panel therefore produces an active power of 4KW but that is insufficient to meet the needs of the non-linear load which requires 9KW (Ppv < P_L). Thus, the AC grid provides the required 5KW of power (P_G >0), and the non-linear load is fed in this case by both sources: the solar panel and the AC grid (P_L = Ppv+ P_G).
- From 0.6 s to 0.9 s: On the one hand, the ignition angle of the nonlinear load abruptly changes from 0° to 90° and the required power decreases to P_L =359W. On the other hand, the irradiation level raises from 200 to 600 W/m2.

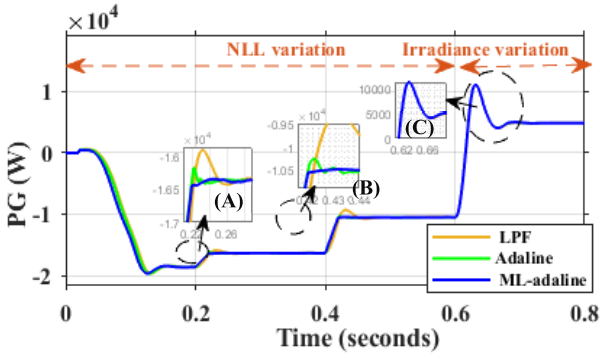

FIGURE 27. Grid power waveform under varying NLL and irradiance profile using P&O with different harmonics extraction strategies.

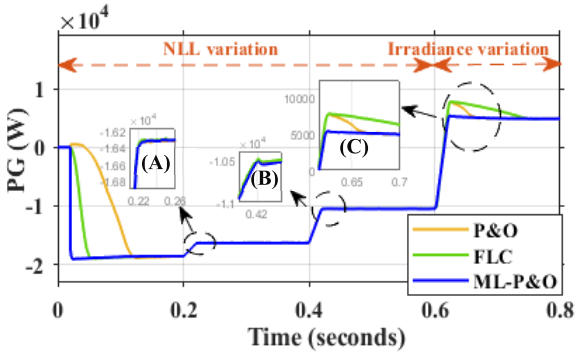

FIGURE 28. Grid power waveform under varying NLL and irradiance profile using Adaline extraction strategy with different MPPT methods.

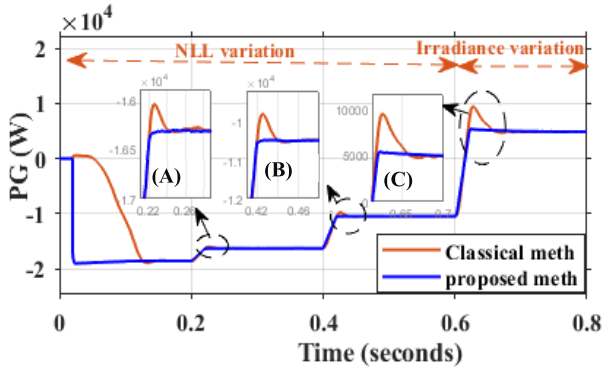

FIGURE 29. Grid power waveform under varying NLL and irradiance profile.

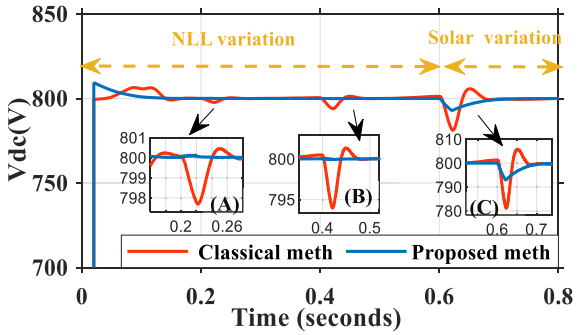

FIGURE 30. The DC voltage waveform under varying NLL and irradiance profile.

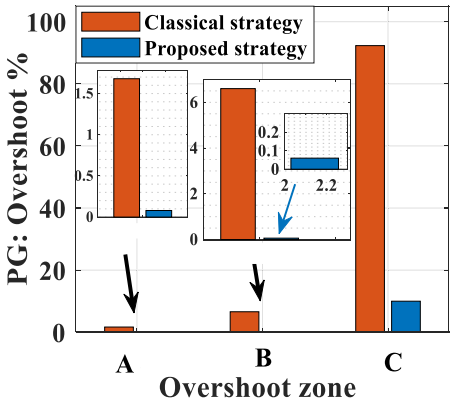

FIGURE 31. Grid power overshoot under NLL or irradiance variation.

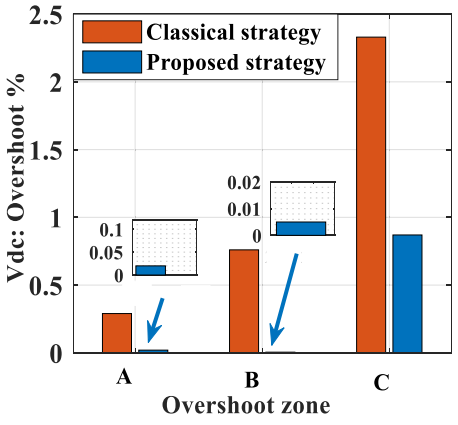

FIGURE 32. DC voltage overshoot under NLL or irradiance variation.

Consequently, the active photovoltaic power production increases up to 12KW and then becomes higher than non-linear load's request (Ppv > P_L). The PVSAPF therefore supplies the active power to the non-linear load and injects the surplus into the AC grid (P_G =-11641W <0; Ppv = P_L+P_G).

As shown in Figures 33.c, Figure 33.d and Figure 33.e, in addition to active power generation, the proposed ML-based system successfully guarantees a sinusoidal waveform of the grid current as well as reactive power compensation, demonstrating its potential as a multi-functional device for compensating harmonics and achieving unity power factor despite the existence of the nonlinear load (Q_G = 0VAR; Q_L = QPVSAPF).

Furthermore, It can be mentioned from Figure 33.e, that the grid current waveform is in phase opposition with the grid voltage when Ppv > PG and the sign of the active grid power is negative (P_G < 0). When the Ppv is lower than PL, the grid

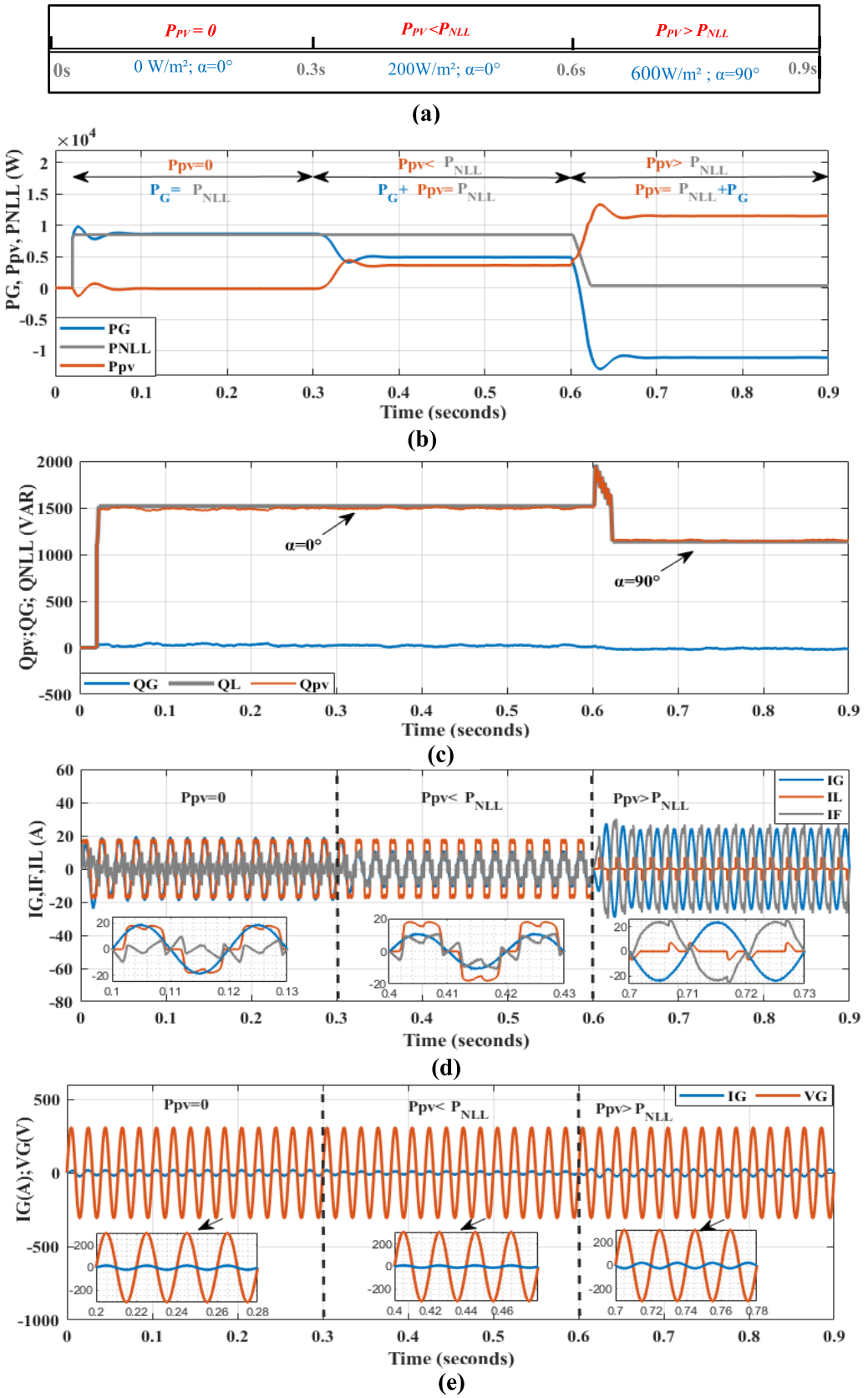

FIGURE 33. PVSAPF performances under three scenarios.

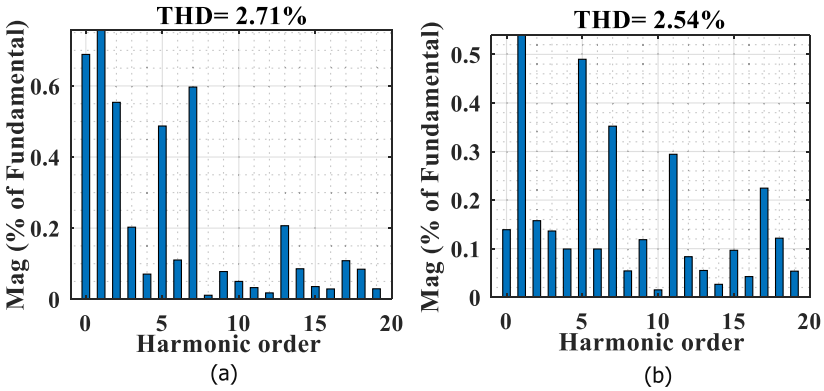

FIGURE 34. PV-SAPF THD performance (E = 0W/m2; σ = 0degrees): a-Classical strategy. b-Proposed ML-based strategy.

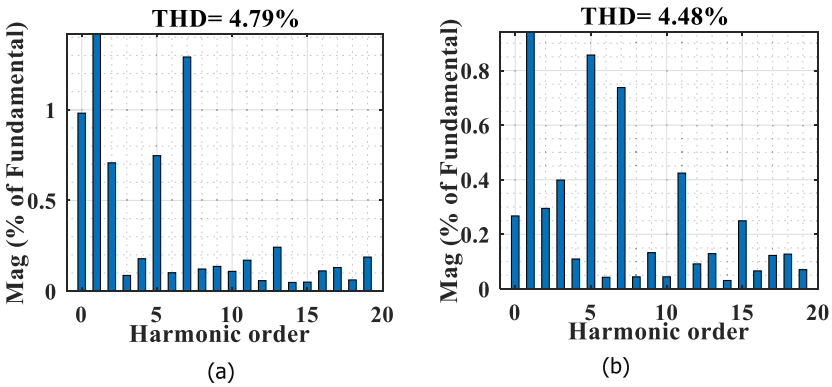

FIGURE 35. PV-SAPF THD performance (E = 200W/m2; σ = 20degrees): a-Classical strategy. b-Proposed ML-based strategy.

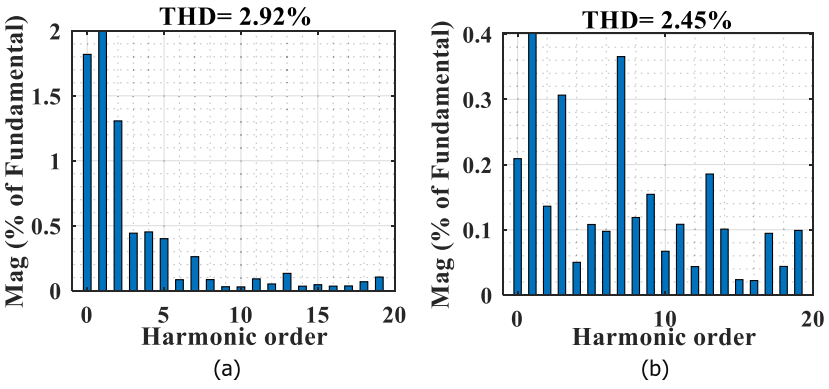

FIGURE 36. PV-SAPF THD performance (E = 600W/m2; σ = 90degrees): a-Classical strategy. b-Proposed ML-based strategy.

current waveform is in phase with the supply voltage and the sign of the grid active power is positive ($P_G > 0$).

The harmonic spectra of the grid current for the three selected operating points, achieved with the traditional PQ approach and with the proposed ML-based Adaline neural PQ design are presented in Figure 34, Figure 35 end Figure 36. TABLE 8 recapitulates the THD values from the discrete Fourier transform (DFT). It can be clearly observed from Figure.37 that the proposed ML-based approach outperforms the remaining ones in all three scenarios. The total harmonic distortion depicted in Figure.38 is performed within the limits prescribed by IEEE-519 using the proposed ML-based PVS-APF system, under load variation, contrary to that obtained by the conventional one.

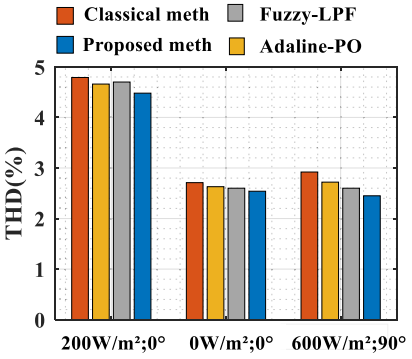

FIGURE 37. THD comparison in all three scenarios.

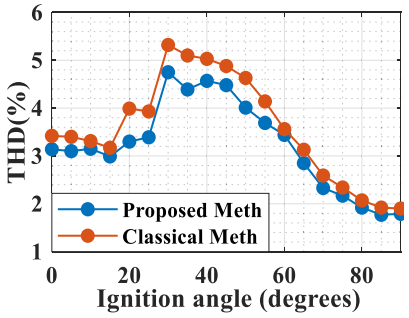

FIGURE 38. THD under variable nonlinear load (1000w/m²).

VI. CONCLUSION

This work affords a significant improvement in maximum power tracking and harmonics detection for PVSAPF system command. In fact, two novel ML based algorithms, named 'SVM regression P& O-MPPT' and 'SVM regression-Adaline NPQ strategy' have been designed. The initialized duty cycle and weights of ADALINE, as predicted outputs of SVM regression blocks, allow fast response on MPP tracking and DC active power component identification, respectively. Further, the ability of the proposed algorithms to work with a small fixed step for MPPT and with a small learning rate parameter in the compensating strategy guarantees an accurate steady-state response. The supremacy of both new techniques is proved by comparison with other conventional and intelligent existing ones. The results confirmed that:

- the SVM regression P&O-MPPT algorithm reaches better solar energy production than other existing algorithms (The average PV energy losses decreased to 99% with the proposed strategy against 72.6% with the FLC based one, compared to the average PV energy losses when the conventional P&O-MPPT algorithm is used). This allows this machine learning based MPPT algorithm to become an attractive and powerful technique for solar energy harvesting, especially when adopting distributed MPPT configurations.

- the new weights updating technique guarantees an accurate

TABLE 9. System parameters in simulation.

Photovoltaic Array	Maximun Power	227.92W
	Open circuit voltage Voc	37.8V
	Short circuit current Isc	8.3A
	Ns ; Np	8 ; 11
DC/DC converter	Inductor	0.45mH
	input capacitor bank	600µF
	output capacitor bank	3500µF
	PWM switching frequency	2KHz
DC/AC converter	DC-link voltage	800V
	DC-link capacitor	3500µF
	Coupling inductor LF	5mH
Utility	Voltage	220V
	Frequency	50Hz
	Rs,Ls	ideal
Nonlinear Load	R; L	30Ω; 0.15mH

DC active power component extraction together with minor oscillations and speed convergence (reduction of the initial error of extraction up to 88%).

- The combination of both new algorithms constitutes an interesting PVSAPF control strategy in terms of power quality enhancement, reactive power compensation and THD decrease whatever the variation of NLL parameters and irradiance levels.

APPENDIX A
SVM REGRESSION-P&O APPROACH: STABILITY PROOF

The Lyapunov function is a positive scalar function for the system state variables. According to the Lyapunov function, the variable structure mode control requests that

$$V = \frac{1}{2}S^2 > 0; \quad \dot{V} = S\frac{dS}{dt} = S\dot{S} < 0 \tag{A1}$$

whereas,

$$S = \frac{\partial P}{\partial V_p} = N_p I_{ph} - N_p I_{rs}\left(exp\left(AV_p\right) - 1\right) - N_p I_{rs} A exp(AV_p)V_p \tag{A2}$$

where $A = \frac{q}{n\beta T_C}\frac{1}{n_s N_s}$.

It is easy to find, from the equation (A2), the following equation (A3)

$$\dot{S} = -N_p I_{rs} A\left[exp\left(AV_p\right) + \left(1 + AV_p\right) exp\left(AV_p\right)\right]\dot{V}_p \tag{A3}$$

First duty cycle is initialized by the predicted output of the SVM regression block.

$$D_{0-MPP} = D_{0-ML} \tag{A4}$$

At the next itteration,

if S >0; based on the new algorithm which switches to P&O:

$$D_{MPP}(k) = D_{0ML} - \Delta D_{P\&O} \tag{A5}$$

$\dot{D} < 0 => \dot{V}p > 0$ (the duty cycle is always opposite to the rate in the voltage)

$$\dot{S} = -A\dot{V}p < 0, => S\dot{S} < 0 \tag{A6}$$

if S < 0; based on the new algorithm which switches to P&O:

$$D_{MPP}(k) = D_{MPP}(k-1) + \Delta D_{P\&O} = D_{0ML} + \Delta D_{P\&O}$$
$$\dot{D} > 0 => \dot{V}p < 0 \tag{A7}$$
$$\dot{S} = -A\dot{V}p > 0, => S\dot{S} < 0 \tag{A8}$$

At the next itteration,

if S > 0; the algorithm is still at P&O the reach accurately MPP:

$$D_{MPP}(k) = D_{MPP}(k-1) - \Delta D_{P\&O}$$
$$\dot{D} < 0 => \dot{V}p > 0 \tag{A9}$$
$$\dot{S} = -A\dot{V}p < 0, \quad => S\dot{S} < 0 \tag{A10}$$

if S < 0; the algorithm is still at P&O the reach accurately MPP:

$$D_{MPP}(k) = D_{MPP}(k-1) + \Delta D_{P\&O}$$
$$\dot{D} > 0 => \quad \dot{V}p < 0 \tag{A11}$$
$$\dot{S} = -A\dot{V}p > 0, \quad => S\dot{S} < 0 \tag{A12}$$

It can be concluded that the system may reach global stability, If the E and/or T parameters change, the duty cycle is again reset by the SVM regression block by $D_{MPP}(k) = D_{MPP}(k\text{-}1) + \Delta D_{ML}$ and the similar stability reasoning is repeated.

APPENDIX B
SVM REGRESSION-ADALINE NEURAL PQ APPROACH: STABILITY PROOF

The update laws of weights used in our study is as follows

$$\begin{cases} W(k+1) = (1-\Psi).W_{ML} + \Psi(W(k) + \mu.e(k).X(k)) \\ \Delta\alpha = 0 \rightarrow \Psi = 1 \\ \Delta\alpha \neq 0 \rightarrow \Psi = 0 \end{cases} \tag{B1}$$

Choose the Lyapunov function as follows: Let the positive definite discrete Lyapunov function is given by:

$$L(k) = \frac{1}{2}e(k)^2 \tag{B2}$$

Now, L (k) is nonzero and positive as long as e (k) is nonzero. For the discrete-time system, stability is guaranteed if

$$\Delta L(k) = L(k+1) - L(k) < 0 \tag{B3}$$

Eq. B3 can be written as follows

$$\Delta L(k) = \frac{1}{2}\Delta e(k)^2 = \frac{1}{2}\left(e(k+1)^2 - e(k)^2\right)$$
$$= \frac{1}{2}(e(k+1) + e(k))(e(k+1) - e(k)) \tag{B4}$$

Using Taylor series expansion, Eq. B5 is obtained:

$$e(k+1) = e(k) + \frac{\partial e(k)}{\partial w(k)}\Delta w(k) \tag{B5}$$

Substituting (B5) into (B4), the derivative of the Lyapunov function is obtained as follows:

$$\Delta L(k) = \frac{1}{2}\left(\frac{\partial e(k)}{\partial w(k)}\Delta w(k) + 2e(k)\right)\frac{\partial e(k)}{\partial w(k)}\Delta w(k) \tag{B6}$$
$$\Delta L(k) = \frac{1}{2}(\Delta e(k) + 2e(k))\Delta e(k) \tag{B7}$$

where

$$\Delta e(k) = e(k+1) - e(k) = \frac{\partial e(k)}{\partial w(k)}\Delta w(k) \tag{B8}$$

Equation (B7) can be rewritten as follows:

$$\frac{1}{2}\Delta e(k)^2 + e(k)\,\Delta e(k) - \Delta L(k) = 0 \tag{B9}$$

Equation (B9) is the second-order equation of $\Delta e(k)$. This equation has a unique solution if the equation (B10) is satisfied:

$$e(k)^2 + 2\Delta L = 0 \tag{B10}$$

Equation (B10) leads to the following result:

$$\Delta L = -\frac{1}{2}e(k)^2 < 0 \tag{B11}$$

Inequation (B11) implies that the closed system is stable, and the estimation errors converge to zero according to the Lyapunov theorem.

REFERENCES

[1] W. U. Rehman, A. R. Bhatti, A. B. Awan, I. A. Sajjad, A. A. Khan, R. Bo, S. S. Haroon, S. Amin, I. Tlili, and O. Oboreh-Snapps, "The penetration of renewable and sustainable energy in Asia: A state-of-the-art review on net-metering," *IEEE Access*, vol. 8, pp. 170364–170388, 2020, doi: 10.1109/ACCESS.2020.3022738.

[2] M. M. V. Cantarero, "Of renewable energy, energy democracy, and sustainable development: A roadmap to accelerate the energy transition in developing countries," *Energy Res. Social Sci.*, vol. 70, Dec. 2020, Art. no. 101716, doi: 10.1016/j.erss.2020.101716.

[3] I. C. Nunesa and M. Catalão-Lopesa, "The impact of oil shocks on innovation for alternative sources of energy: Is there an asymmetric response when oil prices go up or down?" *J. Commodity Markets*, vol. 19, Sep. 2020, Art. no. 100108, doi: 10.1016/j.jcomm.2019.100108.

[4] R. M. Elavarasan, G. M. Shafiullah, S. Padmanaban, N. M. Kumar, A. Annam, A. M. Vetrichelvan, L. Mihet-Popa, and J. B. Holm-Nielsen, "A comprehensive review on renewable energy development, challenges, and policies of leading Indian states with an international perspective," *IEEE Access*, vol. 8, pp. 74432–74457, 2020, doi: 10.1109/ACCESS.2020.2988011.

[5] J. F. do Nascimento Neto, A. J. da Mota, R. A. Roque, W. Heinrichs-Caldas, and W. P. Tadei, "Analysis of the transcription of genes encoding heat shock proteins (hsp) in *Aedes aegypti* Linnaeus, 1762 (Diptera: Culicidae), maintained under climatic conditions provided by the IPCC (intergovernmental panel on climate change) for the year 2100," *Infection, Genet. Evol.*, vol. 86, Dec. 2020, Art. no. 104626, doi: 10.1016/j.meegid.2020.104626.

[6] H. Neofytou, A. Nikas, and H. Doukas, "Sustainable energy transition readiness: A multicriteria assessment index," *Renew. Sustain. Energy Rev.*, vol. 131, Oct. 2020, Art. no. 109988, doi: 10.1016/j.rser.2020.109988.

[7] K. Saidi and A. Omri, "Reducing CO_2 emissions in OECD countries: Do renewable and nuclear energy matter?" *Prog. Nucl. Energy*, vol. 126, Aug. 2020, Art. no. 103425, doi: 10.1016/j.pnucene.2020.103425.

[8] P. R. Brown and F. M. O'Sullivan, "Spatial and temporal variation in the value of solar power across United States electricity markets," *Renew. Sustain. Energy Rev.*, vol. 121, Apr. 2020, Art. no. 109594, doi: 10.1016/j.rser.2019.109594.

[9] V. Ramasamy, D. Feldman, J. Desai, and R. Margolis, "U.S. solar photovoltaic system and energy storage cost benchmarks: Q1 2021," NREL, Golden, CO, USA, Tech. Rep. NREL/TP-7A40-80694, Nov. 2021.

[10] K. N. Nwaigwe, P. Mutabilwa, and E. Dintwa, "An overview of solar power (PV systems) integration into electricity grids," *Mater. Sci. Energy Technol.*, vol. 2, no. 3, pp. 629–633, Dec. 2019, doi: 10.1016/j.mset.2019.07.002.

[11] International Renewable Energy Agency. (Apr. 2021). *Renewable Capacity Statistics 2021*. [Online]. Available: https://www.irena.org/publications/2021/March/Renewable-Capacity-Statistics-2021

[12] International Renewable Energy Agency. (Apr. 2022). *Renewable Capacity Statistics 2022*. [Online]. Available: https://www.irena.org/publications/2022/Apr/Renewable-Capacity-Statistics-2022

[13] K. Zeb, W. Uddin, M. A. Khan, Z. Ali, M. U. Ali, N. Christofides, and H. J. Kim, "A comprehensive review on inverter topologies and control strategies for grid connected photovoltaic system," *Renew. Sustain. Energy Rev.*, vol. 94, pp. 1120–1141, Oct. 2018, doi: 10.1016/j.rser.2018.06.053.

[14] W. Jing, C. H. Lai, W. S. H. Wong, and M. L. D. Wong, "A comprehensive study of battery-supercapacitor hybrid energy storage system for standalone PV power system in rural electrification," *Appl. Energy*, vol. 224, pp. 340–356, Aug. 2018, doi: 10.1016/j.apenergy.2018.04.106.

[15] M. Shafiullah, S. D. Ahmed, and F. A. Al-Sulaiman, "Grid integration challenges and solution strategies for solar PV systems: A review," *IEEE Access*, vol. 10, pp. 52233–52257, 2022, doi: 10.1109/ACCESS.2022.3174555.

[16] M. Bajaj and A. K. Singh, "Grid integrated renewable DG systems: A review of power quality challenges and state-of-the-art mitigation techniques," *Int. J. Energy Res.*, vol. 44, no. 1, pp. 26–69, 2020, doi: 10.1002/er.4847.

[17] J. Gong, D. Li, T. Wang, W. Pan, and X. Ding, "A comprehensive review of improving power quality using active power filters," *Electr. Power Syst. Res.*, vol. 199, Oct. 2021, Art. no. 107389, doi: 10.1016/j.epsr.2021.107389.

[18] R. Chaurasiya and G. P. Rathor, "Simulation of adaptive hybrid shunt active power filter under non-linear load to improve power quality," *Int. J. Electron. Commun. Comput. Eng.*, vol. 12, no. 5, pp. 1–9, Sep. 2021.

[19] R. Kanagavel and V. Indragandhi, "Current control techniques of single phase shunt active power filter—A review," *IOP Conf. Ser., Mater. Sci. Eng.*, vol. 623, no. 1, Oct. 2019, Art. no. 012007, doi: 10.1088/1757-899x/623/1/012007.

[20] D. Buła, D. Grabowski, and M. Macikażek, "A review on optimization of active power filter placement and sizing methods," *Energies*, vol. 15, no. 3, p. 1175, Feb. 2022, doi: 10.3390/en15031175.

[21] F. F. Ahmad, C. Ghenai, A. K. Hamid, and M. Bettayeb, "Application of sliding mode control for maximum power point tracking of solar photovoltaic systems: A comprehensive review," *Annu. Rev. Control.*, vol. 49, pp. 173–196, Jul. 2020, doi: 10.1016/j.arcontrol.2020.04.011.

[22] S. H. Hanzaei, S. A. Gorji, and M. Ektesabi, "A scheme-based review of MPPT techniques with respect to input variables including solar irradiance and PV arrays' temperature," *IEEE Access*, vol. 8, pp. 182229–182239, 2020, doi: 10.1109/ACCESS.2020.3028580.

[23] A. Ali, K. Almutairi, S. Padmanaban, V. Tirth, S. Algarni, K. Irshad, S. Islam, H. Zahir, M. Shafiullah, and M. Z. Malik, "Investigation of MPPT techniques under uniform and non-uniform solar irradiation condition—A retrospection," *IEEE Access*, vol. 8, pp. 127368–127392, 2020, doi: 10.1109/ACCESS.2020.3007710.

[24] S. Motahhir, A. El Hammoumi, and A. El Ghzizal, "The most used MPPT algorithms: Review and the suitable low-cost embedded board for each algorithm," *J. Cleaner Prod.*, vol. 246, Feb. 2020, Art. no. 118983, doi: 10.1016/j.jclepro.2019.118983.

[25] M. Y. Javed, A. F. Mirza, A. Hasan, S. T. H. Rizvi, Q. Ling, M. M. Gulzar, M. U. Safder, and M. Mansoor, "A comprehensive review on a PV based system to harvest maximum power," *Electronics*, vol. 8, no. 12, p. 1480, Dec. 2019, doi: 10.3390/electronics8121480.

[26] V. Jately, B. Azzopardi, J. Joshi, B. Venkateswaran V, A. Sharma, and S. Arora, "Experimental analysis of hill-climbing MPPT algorithms under low irradiance levels," *Renew. Sustain. Energy Rev.*, vol. 150, Oct. 2021, Art. no. 111467, doi: 10.1016/j.rser.2021.111467.

[27] A. K. Gupta, R. K. Pachauri, T. Maity, Y. K. Chauhan, O. P. Mahela, B. Khan, and P. K. Gupta, "Effect of various incremental conductance MPPT methods on the charging of battery load feed by solar panel," *IEEE Access*, vol. 9, pp. 90977–90988, 2021, doi: 10.1109/ACCESS.2021.3091502.

[28] M. N. Ali, K. Mahmoud, M. Lehtonen, and M. M. F. Darwish, "An efficient fuzzy-logic based variable-step incremental conductance MPPT method for grid-connected PV systems," *IEEE Access*, vol. 9, pp. 26420–26430, 2021, doi: 10.1109/ACCESS.2021.3058052.

[29] U. Yilmaz, A. Kircay, and S. Borekci, "PV system fuzzy logic MPPT method and PI control as a charge controller," *Renew. Sustain. Energy Rev.*, vol. 81, pp. 994–1001, Jan. 2018, doi: 10.1016/j.rser.2017.08.048.

[30] C. G. Villegas-Mier, J. Rodriguez-Resendiz, J. M. Álvarez-Alvarado, H. Rodriguez-Resendiz, A. M. Herrera-Navarro, and O. Rodríguez-Abreo, "Artificial neural networks in MPPT algorithms for optimization of photovoltaic power systems: A review," *Micromachines*, vol. 12, no. 10, p. 1260, Oct. 2021, doi: 10.3390/mi12101260.

[31] E. D. Obando, S. X. Carvajal, and J. Pineda Agudelo, "Solar radiation prediction using machine learning techniques: A review," *IEEE Latin Amer. Trans.*, vol. 17, no. 4, pp. 684–697, Apr. 2019, doi: 10.1109/TLA.2019.8891934.

[32] A. Samanta, S. Chowdhuri, and S. S. Williamson, "Machine learning-based data-driven fault detection/diagnosis of lithium-ion battery: A critical review," *Electronics*, vol. 10, no. 11, p. 1309, May 2021, doi: 10.3390/electronics10111309.

[33] S. R. Das, P. K. Ray, A. K. Sahoo, S. Ramasubbareddy, T. S. Babu, N. M. Kumar, R. M. Elavarasan, and L. Mihet-Popa, "A comprehensive survey on different control strategies and applications of active power filters for power quality improvement," *Energies*, vol. 14, no. 15, p. 4589, Jul. 2021, doi: 10.3390/en14154589.

[34] Q. Lv, F. Zhao, Z. Guo, and X. Zong, "A review of research on power system harmonic detection and its suppression methods," in *Proc. ITNEC*, Jun. 2020, pp. 1495–1500. [Online]. Available: https://ieeexplore.ieee.org/document/9084832

[35] A. A. Imam, R. S. Kumar, and Y. A. Al-Turki, "Modeling and simulation of a pi controlled shunt active power filter for power quality enhancement based on P-Q theory," *Electronics*, vol. 9, no. 4, p. 637, Apr. 2020, doi: 10.3390/electronics9040637.

[36] P. Khetarpal and M. M. Tripathi, "A critical and comprehensive review on power quality disturbance detection and classification," *Sustain. Comput., Informat. Syst.*, vol. 28, Dec. 2020, Art. no. 100417, doi: 10.1016/j.suscom.2020.100417.

[37] M. M. Zainuri, M. M. Radzi, A. C. Soh, N. Mariun, N. A. Rahim, J. Teh, and C.-M. Lai, "Photovoltaic integrated shunt active power filter with simpler ADALINE algorithm for current harmonic extraction," *Energies*, vol. 11, no. 5, p. 1152, May 2018, doi: 10.3390/en11051152.

[38] S. Janpong, K. Areerak, and K. Areerak, "Harmonic detection for shunt active power filter using ADALINE neural network," *Energies*, vol. 14, no. 14, p. 4351, Jul. 2021, doi: 10.3390/en14144351.

[39] L. Alhafadhi and J. Teh, "Advances in reduction of total harmonic distortion in solar photovoltaic systems: A literature review," *Int. J. Energy Res.*, vol. 44, no. 4, pp. 2455–2470, 2020, doi: 10.1002/er.5075.

[40] K. Parand, A. A. Aghaei, M. Jani, and A. Ghodsi, "A new approach to the numerical solution of Fredholm integral equations using least squares-support vector regression," *Math. Comput. Simul.*, vol. 180, pp. 114–128, Feb. 2021, doi: 10.1016/j.matcom.2020.08.010.

[41] A. F. Al-Anazi and I. D. Gates, "Support vector regression for porosity prediction in a heterogeneous reservoir: A comparative study," *Comput. Geosci.*, vol. 36, no. 12, pp. 1494–1503, Dec. 2010, doi: 10.1016/j.cageo.2010.03.022.

[42] Z. Ceylan, "Estimation of municipal waste generation of Turkey using socio-economic indicators by Bayesian optimization tuned Gaussian process regression," *Waste Manage. Res.*, vol. 38, no. 8, pp. 840–850, Mar. 2020, doi: 10.1177/0734242x20906877.

[43] S. Thomas, G. N. Pillai, and K. Pal, "Prediction of peak ground acceleration using ϵ-SVR, ν-SVR and Ls-SVR algorithm," *Geomatics, Natural Hazards Risk*, vol. 8, no. 2, pp. 177–193, Apr. 2016, doi: 10.1080/19475705.2016.1176604.

[44] V. H. Quej, J. Almorox, J. A. Arnaldo, and L. Saito, "ANFIS, SVM and ANN soft-computing techniques to estimate daily global solar radiation in a warm sub-humid environment," *J. Atmos. Sol.-Terr. Phys.*, vol. 155, pp. 62–70, Mar. 2017, doi: 10.1016/j.jastp.2017.02.002.

[45] S. Ekız, and P. Erdoğmuş, "Comparative study of heart disease classification," in *Proc. EBBT*, Apr. 2017, pp. 1–4. [Online]. Available: https://ieeexplore.ieee.org/abstract/document/7956761

[46] Y. Karaca and C. Cattani, "Model estimation with SVM kernel types for cognitive diagnostics," *Adv. Math. Models Appl.*, vol. 4, no. 1, pp. 5–14, Apr. 2019.

[47] S. Putatunda and K. Rama, "A modified Bayesian optimization based hyper-parameter tuning approach for extreme gradient boosting," in *Proc. ICINPRO*, Dec. 2020, pp. 1–6. [Online]. Available: https://ieeexplore.ieee.org/document/9092025

[48] S. S. Hossain, B. V. Ayodele, S. S. Ali, C. K. Cheng, and S. I. Mustapa, "Comparative analysis of support vector machine regression and Gaussian process regression in modeling hydrogen production from waste effluent," *Sustainability*, vol. 14, no. 12, p. 7245, Jun. 2022, doi: 10.3390/su14127245.

[49] M. Beza and M. Bongiorno, "A modified RLS algorithm for online estimation of low-frequency oscillations in power systems," *IEEE Trans. Power Syst.*, vol. 31, no. 3, pp. 1703–1714, May 2016, doi: 10.1109/TPWRS.2015.2439811.

[50] L. Merabet, S. Saad, D. O. Abdeslam, and J. Merckle, "Direct neural method for harmonic currents estimation using adaptive linear element," *Electr. Power Syst. Res.*, vol. 152, pp. 61–70, Nov. 2017, doi: 10.1016/j.epsr.2017.06.018.

[51] B. Singh, S. K. Dube, S. R. Arya, A. Chandra, and K. Al-Haddad, "A comparative study of adaptive control algorithms in distribution static compensator," in *Proc. IECON*, Nov. 2013, pp. 145–150. [Online]. Available: https://ieeexplore.ieee.org/abstract/document/6699126

[52] M. Qasim, P. Kanjiya, and V. Khadkikar, "Optimal current harmonic extractor based on unified ADALINEs for shunt active power filters," *IEEE Trans. Power Electron.*, vol. 29, no. 12, pp. 6383–6393, Dec. 2014, doi: 10.1109/TPEL.2014.2302539.

[53] U. Younas and A. A. Kulaksiz, "Deep learning LSTM-based MPPT control of 100 kW dual stage grid tied solar PV system," *Res. Square*, Feb. 2023, doi: 10.21203/rs.3.rs-2539136/v1.

[54] A. K. Devarakonda, N. Karuppiah, T. Selvaraj, P. K. Balachandran, R. Shanmugasundaram, and T. Senjyu, "A comparative analysis of maximum power point techniques for solar photovoltaic systems," *Energies*, vol. 15, no. 22, p. 8776, Nov. 2022, doi: 10.3390/en15228776.

[55] S. Allahabadi, H. Iman-Eini, and S. Farhangi, "Fast artificial neural network based method for estimation of the global maximum power point in photovoltaic systems," *IEEE Trans. Ind. Electron.*, vol. 69, no. 6, pp. 5879–5888, Jun. 2022, doi: 10.1109/TIE.2021.3094463.

[56] M. S. Karabinaoğlu, B. Çakir, M. E. Başoğlu, A. Kazdaloğlu, and A. Güneroğlu, "Comparison of deep learning and regression-based MPPT algorithms in PV systems," *Turkish J. Electr. Eng. Comput. Sci.*, vol. 30, no. 6, pp. 2319–2338, Jan. 2022, doi: 10.55730/1300-0632.3941.

[57] A. Yadav and A. R. Chowdhury, "Deep *Q* reinforcement learning to improve the MPPT in solar cell," *Adv. Appl. Math. Sci.*, vol. 21, no. 5, pp. 2781–2793, Mar. 2022.

[58] A. Azzam-Jai and M. Ouassaid, "Photovoltaic interfaced shunt active power filter under online-varying parameters based on fuzzy logic controller and adaptive hysteresis band current controller," in *Proc. ICDS*, Oct. 2019, pp. 1–7. [Online]. Available: https://ieeexplore.ieee.org/document/8942282

ASMAE AZZAM JAI received the Diploma degree in electrical engineering from the National School of Electricity and Mechanics (ENSEM), Casablanca, in 2009. She is currently pursuing the Ph.D. degree with the Department of Electrical Engineering, Mohammadia School of Engineering (EMI), Mohamed V University in Rabat, Rabat, Morocco.

From 2010 to 2019, she was a Trainer Engineer with the Office of Vocational Training and Employment Promotion. In 2019, she joined the Department of Electrical Engineering, EMI, Rabat, where she is a Teacher Engineer. Her research interest includes control and optimization of PV-based shunt active power filter.

MOHAMMED OUASSAID (Senior Member, IEEE) received the Diploma of Agrégation degree in electrical engineering from Ecole Nationale Supérieure d'Art et Métiers de Rabat (ex ENSET), Rabat, Morocco, in 1999, the M.Sc.A. and Ph.D. degrees in electrical engineering from the Mohammadia School of Engineers (EMI), Mohamed V University in Rabat, Rabat, in 2002 and 2006, respectively, and the Diploma degree from University's Habilitation, in 2012. From 2008 to 2015, he was a Professor with the National School of Applied Sciences of Safi (ENSA-Safi), Cadi Ayyad University, Marrakesh, Morocco. In 2015, he joined the Department of Electrical Engineering, Mohammadia School of Engineers, Mohammed V University in Rabat, where he is currently a Full Professor. He is also involved in a number of research and teaching projects. He is the author or coauthor of numerous book chapters and articles in refereed journals and international conference proceedings. His main research interests include electrical drives, power systems, control and optimization of renewable energy, integration of wind power and photovoltaic systems, microgrid, and smart grids. He is a member of the IEEE Power and Energy Society.